Comput Mech (2015) 56:421–441
DOI 10.1007/s00466-015-1179-5

ORIGINAL PAPER

Homogenization of soft interfaces in time-dependent hydrodynamic lubrication

G. Kabacaoğlu[1] · **İ. Temizer**[1]

Received: 14 December 2014 / Accepted: 24 June 2015 / Published online: 11 July 2015

Abstract The difficulty behind the unsteady lubrication problem is the oscillation of the film thickness in both position and time. The present study aims to extend the multiscale analysis of lubricated interfaces to the unsteady hydrodynamic lubrication case with deformable random microrough surfaces. For that purpose, the homogenization framework for the time-dependent problem is first presented in a setting that unifies all hydrodynamic lubrication cases. The differences between the periodic commensurate and incommensurate as well as random microrough surfaces are highlighted with numerical investigations. A time averaging method is proposed in order to deliver the effective macroscopic response and its efficacy is discussed for different types of microrough surfaces. Finally, the deformation is implemented through the numerically efficient Taylor assumption at the microscale and the ability of the proposed method to reflect the deformation effects is discussed.

Keywords Soft elastohydrodynamic lubrication · Time-dependent Reynolds equation · Homogenization · Random roughness · Taylor assumption

1 Introduction

Lubrication, action of a viscous fluid between two interacting surfaces, has applications in various fields in order to reduce friction and wear of the surfaces [1,2]. Early lubrication studies focused on the industrial applications [3,4]. There are very recent lubrication studies related to the biological applications as well. The fundamental mechanisms of synovial fluid lubrication in artificial joints have been examined in order to enlighten the tribological problem of failure of metal-on-metal and metal-on-polymer joints (see [5–7]). The reader is referred to [8] for an extensive review on the state of the art of both lubrication and wear models for artificial hip joints. Another biological phenomenon of contact lens wear during blinking is investigated by [9] and an eye is depicted as an example of a lubricated moving system in the human body. Additionally, lubrication and contact mechanics are used as a basis for understanding the tribological process in syringes by [10]. Furthermore, surface engineering is an emerging technology related to lubrication. Various studies have been conducted on optimal surface textures in order to increase the load carrying capacity of bearings (see [11–14]). It is, therefore, important to understand the macroscopic response of such microrough surfaces.

The mathematical model for the lubrication theory has been developed in [3]. The governing equation is called the Reynolds equation which is a second-order elliptic partial differential equation. The equation is derived from the Navier-Stokes equations of motion, based on the assumption that due to the thinness of the fluid film the viscous forces dominate the inertial forces and the pressure change in the out-of-plane direction is negligible. Therefore, a three-dimensional nonlinear problem is reduced to a two-dimensional lubrication problem that is represented by the linear Reynolds equation. Despite the series of underlying assumptions, the Reynolds equation has a reliable predictive capability in its domain of applicability, as demonstrated in Fig. 1a for the classical wedge problem (see Fig. 3). An additional underlying assumption in the Reynolds equation is microscopically smooth surfaces. However, this assumption is invalid in most cases because surfaces are inherently rough and roughness is no longer negligible in compari-

✉ İ. Temizer
temizer@bilkent.edu.tr

[1] Department of Mechanical Engineering, Bilkent University, 06800 Ankara, Turkey

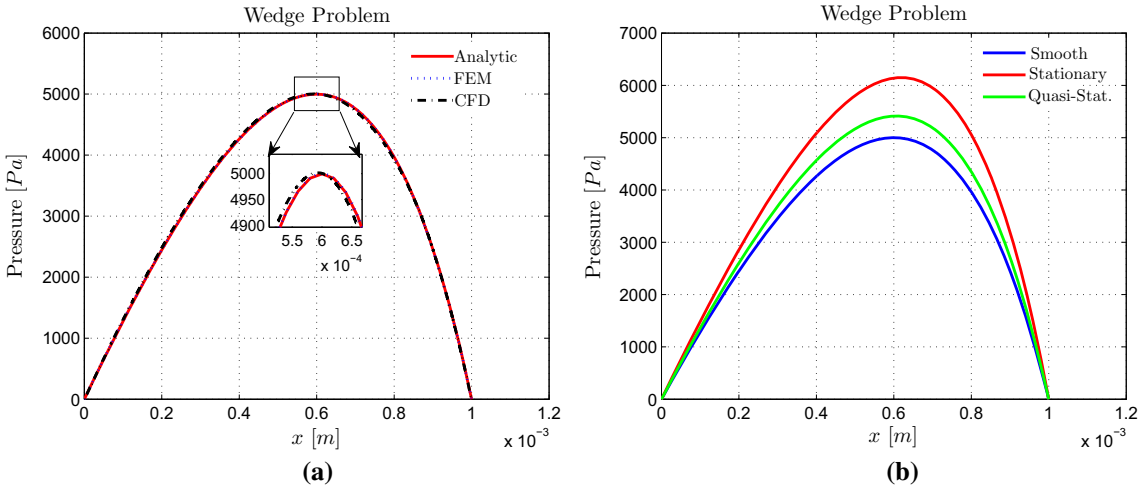

Fig. 1 For the wedge problem depicted on Fig. 3 where the surfaces are assumed to be smooth, the analytic and FEM solutions to the Reynolds equation are compared with the CFD solution (Stokes equation) in (**a**). **b** shows that microscopic roughness under different lubrication cases (see Fig. 2) leads to different homogenized solutions that differ from the solution obtained under the assumption of smooth surfaces. (**a**) Microscopically smooth surfaces. **b** Microscopically rough lower surface

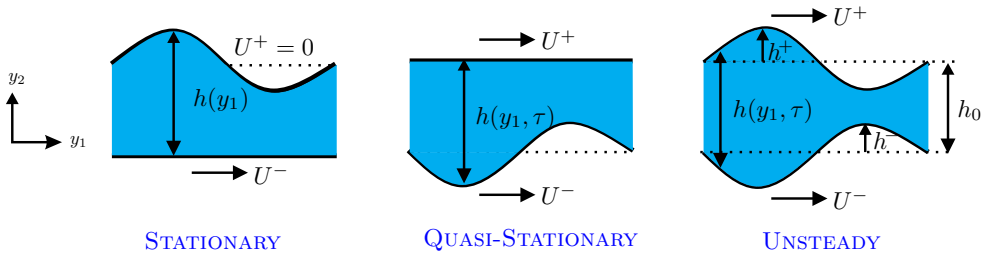

Fig. 2 Based on the roughness and the motion of each surface, the lubrication problem is divided into three cases [15]

son with the small fluid film thickness that is encountered in lubrication. Nevertheless, for a broad range of scenarios (see below), the Reynolds equation is able to reflect well-known roughness effects. This is demonstrated in Fig. 1b where the surface roughness is considered as a sinusoidal function with an amplitude of 0.5 μm. Here, the stationary and the quasi-stationary cases discussed further below are solved in a two-scale setting. Roughness increases the pressure and hence the load bearing capacity. Additionally, this influence depends on whether the moving surface or the stationary surface is rough.

In a pioneering study [15], the lubrication problem is divided into three cases (see Fig. 2) based on the surface roughness and motion. As long as the smooth surface moves and the rough one does not, the problem is called time-independent or *stationary*. On the other hand, when the rough surface is moving the problem becomes dependent on a microscopic time, which is the emphasis of this work: in the *quasi-stationary* case the opposing moving surface is smooth and in the *unsteady* case it is also rough. The methods in the literature to incorporate such roughness effects into the Reynolds equation are divided into three groups in [16]. The simultaneous resolution of all scales of the problem constitutes the *deterministic analysis* and this approach has been followed in [17,18]. *Stochastic analysis*, developed by [19,20] with the influential flow factor method introduced in [21–23] as a particular example, aims to capture the coarse-scale interface response by incorporating fine-scale information. Finally, the third method is known as *two-scale analysis*, an early example being the approach of [24] which can be considered as a precursor to modern homogenization techniques. The widely employed flow factor method is rendered ineffective in the presence of asymmetric roughness (see [25]). Another drawback of this method is that tedious effort is required to obtain the flow factors through flow simulations. On the other hand, the deterministic analysis accurately captures the directional aspect of the roughness as long as a very fine numerical discretization is employed, which may be computationally prohibitive. In this work, the homogenization approach is chosen in order to circumvent both of these difficulties. Homogenization divides the problem into two parts: a microscopic problem (i.e. the roughness

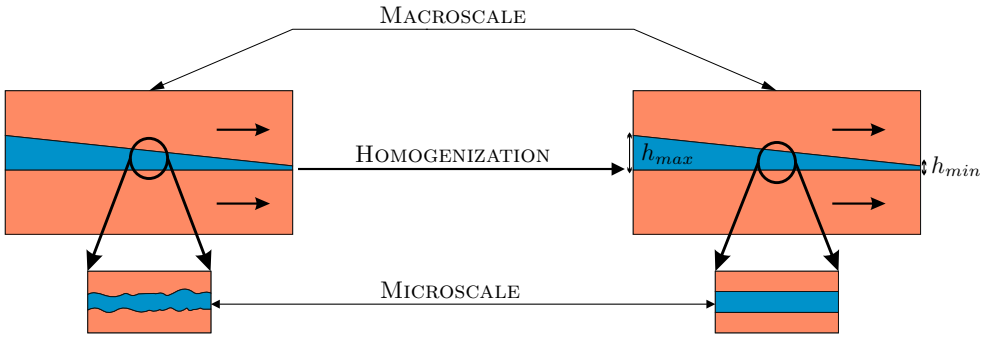

Fig. 3 The homogenization idea for the two-scale lubrication problem in which the heterogeneous surfaces are replaced with microscopically smooth ones. Here, the macroscopic problem is a simple wedge problem with maximum and minimum film thicknesses (h_{max} and h_{min}, respectively) and at the microscale the surfaces can be considered as nominally flat. See Fig. 1 for sample solutions in 1D and Fig. 4 for 2D. In all cases, Dirichlet boundary conditions have been applied on the boundary of the domain by setting the pressure to zero

scale) and a macroscopic problem (i.e. the structural interface scale) (see Fig. 3). An explicit incorporation of those two scales into the lubrication problem was first realized by [24]. Small parameter expansion approach was then used to separate those two scales for the lubrication problem in [26,27]. Within this approach, for the heterogeneous problem the macroscopic response (i.e. the mean pressure) is extracted from the microstructure without any simplification. Therefore, the microstructure of the problem can be either periodic or random, which removes the symmetric roughness requirement of the flow factor method (see [25]).

There are four lubrication regimes where homogenization approaches are of interest. *Mixed* and *boundary lubrication* regimes are used to refer to the cases when the surfaces are partially in contact, which will not be addressed in this work (see [2] for a detailed review). As long as the pressure within the fluid is not sufficiently high to deform the surfaces, the regime is called *hydrodynamic lubrication*; and it is known as *elastohydrodynamic lubrication* when the surfaces are deformed significantly. The homogenization of the hydrodynamic lubrication problem in the stationary case is presented in [28–30]. Analytic bounds for the problem and their comparison with homogenization are studied in [31,32]. The homogenization of the time-dependent lubrication problem is studied in [15,29] in addition to [33]. Bounds for the time-dependent problem is discussed in [34]. The homogenization of the compressible Reynolds equation in the stationary case is studied for modeling a hard disk magnetic storage problem in [35]. It is further generalized and applied for the time-dependent Reynolds equation in [33]. Homogenization is compared with alternative methods in [16,36]. Additionally, the stationary multiscale problem of elastohydrodynamic lubrication is investigated in [37–40].

Since the Reynolds equation is derived based on a series of simplifying assumptions, the validity of the use of the equation at the microscale, specifically in the context of homogenization, has been of interest. For that purpose, two types of roughness regimes are described in the literature. As long as the roughness wavelength to the mean film thickness ratio is large, the regime is classified as Reynolds roughness and the Reynolds equation is applicable. On the contrary, if the ratio is small, the regime is classified as Stokes roughness and reverting to the Stokes equation might be necessary. The limits of the wavelength to the film thickness ratio where the Reynolds equation is valid is investigated in [41–45] for various roughness profiles. On the other hand, the validity of the Reynolds equation is studied from a mathematical perspective in [46] where it is shown that the Stokes equation reduces to the classical Reynolds equation with an effective height in the limit of first the wavelength approaching to zero and then the film thickness as well. On the other hand, the Stokes equation condenses to the homogenized Reynolds equation in the limit of first the film thickness and then the wavelength approaching to zero, essentially describing Reynolds roughness. The microstructures employed in this study have Reynolds roughness, hence the use of Reynolds equation in a two-scale setting can be considered a valid approach.

The literature cited above concerning the homogenization of the Reynolds equation concentrates predominantly on the time-independent case and in the time-dependent cases emphasis has been solely on periodic surfaces with little or no deformation. The aim of the present study is to extend the multiscale analysis of lubricated interfaces to the time-dependent cases with deformable random microrough surfaces. For that purpose, the homogenization framework for the time-dependent lubrication problem is presented in Sect. 2 in a setting that unifies all hydrodynamic lubrication cases. Next, a time averaging method to deliver the effective macroscopic response in the unsteady case is proposed and applied to periodic as well as random microrough surfaces in Sect. 3. Finally, the deformation effects are reflected in the microscale through the numerically efficient Taylor

assumption where the boundary layer deformation is projected uniformly onto the micromechanical sample. In order to investigate the efficiency of the proposed method, the results are compared with the solutions of the problem where the deformation of the microstructure is resolved explicitly using the finite element method (FEM).

2 Homogenization of time-dependent Reynolds equation

2.1 Two-scale expansion in space and time

The homogenization framework for the unsteady lubrication problem was established in [15], which is reviewed in this section. The quasi-stationary and the unsteady cases of the lubrication problem in a macroscopic domain Ω are governed by the incompressible time-dependent Reynolds equation

$$\nabla\cdot\left(\frac{h_\varepsilon(\mathbf{x}_\varepsilon,t_\varepsilon)^3}{12\mu}\nabla p_\varepsilon(\mathbf{x}_\varepsilon,t_\varepsilon)\right) = \frac{1}{2}\mathbf{U}\cdot\nabla h_\varepsilon(\mathbf{x}_\varepsilon,t_\varepsilon)+\frac{\partial h_\varepsilon(\mathbf{x}_\varepsilon,t_\varepsilon)}{\partial t_\varepsilon} \tag{2.1}$$

where $p_\varepsilon(\mathbf{x}_\varepsilon,t_\varepsilon)$ is the pressure, $h_\varepsilon(\mathbf{x}_\varepsilon,t_\varepsilon)$ is the fluid film thickness, μ is the kinematic viscosity, and $\mathbf{U}=\mathbf{U}^+ + \mathbf{U}^-$ (see Fig. 2). Here, the microscale is the surface roughness scale and it is separated from the macroscale by the factor ε which is proportional to the roughness wavelength. The deterministic position vector $\mathbf{x}_\varepsilon$ and time t_ε can then be expressed in a two-scale setting as

$$\mathbf{x}_\varepsilon=\mathbf{x}+\varepsilon\mathbf{y},\quad t_\varepsilon=t+\varepsilon\tau \tag{2.2}$$

where $\mathbf{x}/\mathbf{y}$ is the macroscopic/microscopic position vector and t/τ is the macroscopic/microscopic time. It follows that the relevant gradients are

$$\frac{\partial}{\partial\mathbf{x}_\varepsilon}=\frac{\partial}{\partial\mathbf{x}}+\frac{1}{\varepsilon}\frac{\partial}{\partial\mathbf{y}},\quad \frac{\partial}{\partial t_\varepsilon}=\frac{\partial}{\partial t}+\frac{1}{\varepsilon}\frac{\partial}{\partial\tau}. \tag{2.3}$$

The film thickness is assigned a relatively general two-scale representation in the form

$$\begin{aligned}h_\varepsilon(\mathbf{x}_\varepsilon,t_\varepsilon)&=h(\mathbf{x},t,\mathbf{y},\tau)\\&=h_0(\mathbf{x},t)+h^+(\mathbf{y}-\mathbf{U}^+\tau)-h^-(\mathbf{y}-\mathbf{U}^-\tau)\end{aligned} \tag{2.4}$$

where $h_0(\mathbf{x},t)$ is the mean (macroscopic) film thickness while h^+ and h^- are two functions with zero mean that describe the microscopic roughness topographies of the surfaces (see Fig. 2).

Assuming ε is small, one proposes an asymptotic expansion of the pressure in terms of ε:

$$\begin{aligned}p_\varepsilon(\mathbf{x}_\varepsilon,t_\varepsilon)&=p(\mathbf{x},t,\mathbf{y},\tau)\\&=p_0(\mathbf{x},t,\mathbf{y},\tau)+\varepsilon p_1(\mathbf{x},t,\mathbf{y},\tau)\\&\quad+\varepsilon^2 p_2(\mathbf{x},t,\mathbf{y},\tau)+\mathcal{O}(\varepsilon^3).\end{aligned} \tag{2.5}$$

Here p_1 and p_2 are periodic functions of $\mathbf{y}$ on a microscopic domain $\mathcal{Y}$ and of τ in time with a period $\mathcal{T}$. Substituting (2.3) and (2.5) into (2.1), and defining the differential operators

$$\mathcal{A}_0=\nabla_\mathbf{x}\cdot\left(\frac{h^3}{12\mu}\nabla_\mathbf{x}\right), \tag{2.6a}$$

$$\mathcal{A}_1=\nabla_\mathbf{y}\cdot\left(\frac{h^3}{12\mu}\nabla_\mathbf{x}\right)+\nabla_\mathbf{x}\cdot\left(\frac{h^3}{12\mu}\nabla_\mathbf{y}\right), \tag{2.6b}$$

$$\mathcal{A}_2=\nabla_\mathbf{y}\cdot\left(\frac{h^3}{12\mu}\nabla_\mathbf{y}\right), \tag{2.6c}$$

the heterogeneous Reynolds equation is expressed as follows

$$\begin{aligned}&\left(\mathcal{A}_0+\varepsilon^{-1}\mathcal{A}_1+\varepsilon^{-2}\mathcal{A}_2\right)\left(p_0+\varepsilon p_1+\varepsilon^2 p_2+\ldots\right)\\&\quad=\frac{1}{2}\mathbf{U}\cdot\left[(\nabla_\mathbf{x}+\varepsilon^{-1}\nabla_\mathbf{x})h\right]+\left(\frac{\partial}{\partial t}+\varepsilon^{-1}\frac{\partial}{\partial\tau}\right)h.\end{aligned} \tag{2.7}$$

Gathering the terms of equal powers of $\varepsilon\to 0$ delivers three equations for ε^{-2}, ε^{-1} and ε^0:

$$\mathcal{A}_2 p_0=0, \tag{2.8a}$$

$$\mathcal{A}_1 p_0+\mathcal{A}_2 p_1=\frac{1}{2}\mathbf{U}\cdot\nabla_\mathbf{y}h+\frac{\partial h}{\partial\tau}, \tag{2.8b}$$

$$\mathcal{A}_0 p_0+\mathcal{A}_1 p_1+\mathcal{A}_2 p_2=\frac{1}{2}\mathbf{U}\cdot\nabla_\mathbf{x}h+\frac{\partial h}{\partial t}. \tag{2.8c}$$

From the first Eq. (2.8a), it is obtained that the macroscale pressure p_0 is independent of $\mathbf{y}$: $p_0(\mathbf{x},t,\mathbf{y},\tau)=p_0(\mathbf{x},t,\tau)$. In the second Eq. (2.8b), by linearity of the differential equation, the microscale pressure (p_1) is replaced with

$$\begin{aligned}p_1(\mathbf{x},t,\mathbf{y},\tau)=&\frac{\partial p_0}{\partial x_1}w_1(\mathbf{x},t,\mathbf{y},\tau)+\frac{\partial p_0}{\partial x_2}w_2(\mathbf{x},t,\mathbf{y},\tau)\\&+w_3(\mathbf{x},t,\mathbf{y},\tau)\end{aligned} \tag{2.9}$$

where w_1, w_2 and w_3 are $\mathcal{Y}$- and $\mathcal{T}$-periodic functions. One then obtains the cell problems

$$\nabla_\mathbf{y}\cdot\left(\frac{h^3}{12\mu}\nabla_\mathbf{y}w_1\right)=-\frac{\partial}{\partial y_1}\left(\frac{h^3}{12\mu}\right), \tag{2.10a}$$

$$\nabla_\mathbf{y}\cdot\left(\frac{h^3}{12\mu}\nabla_\mathbf{y}w_2\right)=-\frac{\partial}{\partial y_2}\left(\frac{h^3}{12\mu}\right), \tag{2.10b}$$

$$\nabla_\mathbf{y}\cdot\left(\frac{h^3}{12\mu}\nabla_\mathbf{y}w_3\right)=\frac{1}{2}\mathbf{U}\cdot\nabla_\mathbf{y}h+\frac{\partial h}{\partial\tau}. \tag{2.10c}$$

Finally, solving the cell problems and taking the cell average $\langle\cdot\rangle=\frac{1}{|\mathcal{Y}|}\int_\mathcal{Y}\cdot\ \mathrm{d}\mathbf{y}$ of the third Eq. (2.8c) delivers the

homogenized equation in the macroscopic domain Ω for the $\mathcal{T}$-periodic macroscopic pressure p_0:

$$\nabla_{\mathbf{x}}\cdot(\mathbf{A}(\mathbf{x},t,\tau)\nabla_{\mathbf{x}}p_0(\mathbf{x},t,\tau))=\nabla_{\mathbf{x}}\cdot\mathbf{b}(\mathbf{x},t,\tau)+\frac{\partial h_0}{\partial t} \quad (2.11)$$

Here, $\langle h\rangle = h_0(\mathbf{x},t)$ has been employed and the homogenized response is reflected through

$$[\mathbf{A}]=\begin{bmatrix}\left\langle\frac{h^3}{12\mu}+\frac{h^3}{12\mu}\frac{\partial w_1}{\partial y_1}\right\rangle & \left\langle\frac{h^3}{12\mu}\frac{\partial w_2}{\partial y_1}\right\rangle\\ \left\langle\frac{h^3}{12\mu}\frac{\partial w_1}{\partial y_2}\right\rangle & \left\langle\frac{h^3}{12\mu}+\frac{h^3}{12\mu}\frac{\partial w_2}{\partial y_2}\right\rangle\end{bmatrix}, \quad (2.12a)$$

$$\{\mathbf{b}\}=\begin{Bmatrix}\left\langle\frac{h}{2}U_1-\frac{h^3}{12\mu}\frac{\partial w_3}{\partial y_1}\right\rangle\\ \left\langle\frac{h}{2}U_2-\frac{h^3}{12\mu}\frac{\partial w_3}{\partial y_2}\right\rangle\end{Bmatrix}=\frac{h_0}{2}\begin{Bmatrix}U_1\\U_2\end{Bmatrix}-\begin{Bmatrix}\left\langle\frac{h^3}{12\mu}\frac{\partial w_3}{\partial y_1}\right\rangle\\ \left\langle\frac{h^3}{12\mu}\frac{\partial w_3}{\partial y_2}\right\rangle\end{Bmatrix}. \quad (2.12b)$$

Remark The microscopic fluid flux $\mathbf{q}$ can be written as follows (see [1])

$$q_1=-\frac{h^3}{12\mu}\left(\frac{\partial p_1}{\partial y_1}+\frac{\partial p_0}{\partial x_1}\right)+\frac{h}{2}U_1, \quad (2.13a)$$

$$q_2=-\frac{h^3}{12\mu}\left(\frac{\partial p_1}{\partial y_2}+\frac{\partial p_0}{\partial x_2}\right)+\frac{h}{2}U_2. \quad (2.13b)$$

After substituting (2.9) into (2.13a) and (2.13b), taking the cell average of the microscopic fluid flux delivers the following expression for the macroscopic fluid flux

$$\mathbf{Q}=\langle\mathbf{q}\rangle=-\mathbf{A}(\mathbf{x},t,\tau)\nabla_{\mathbf{x}}p_0(\mathbf{x},t,\tau)+\mathbf{b}(\mathbf{x},t,\tau) \quad (2.14)$$

which therefore satisfies the macroscopic Reynolds equation (2.11):

$$-\nabla_{\mathbf{x}}\cdot\mathbf{Q}=\frac{\partial h_0}{\partial t}. \quad (2.15)$$

The microscale problems are, by construction, nominally flat even though the macroscale interfaces may be curved. The divergence and the gradient operators in these expressions would then be evaluated accordingly (see [47]).

Remark In this work, time-dependence refers to the presence of the microscopic time τ. Although the variation of the vertical separation h_0 of the surfaces with the macroscopic time t is not considered in the numerical experiments, the presented theory is capable of addressing this case without modification via the macroscopic term $\frac{\partial h_0}{\partial t}$.

2.2 Homogenized coefficient tensors

The term $\frac{\partial h}{\partial\tau}$ in (2.10c) vanishes in the stationary case so that w_3 may be expressed as a linear function of $\mathbf{U}$ without loss of generality: $w_3=-\boldsymbol{\Omega}(\mathbf{x},t,\mathbf{y})\cdot\mathbf{U}$. Note, however, that $\mathbf{U}$ is either equal to $\boldsymbol{U}^+$ or $\boldsymbol{U}^-$, whichever surface is smooth. This splits equation (2.10c) into two equations for the two components Ω_1 and Ω_2 of $\boldsymbol{\Omega}$. Substitution of $w_3=-\boldsymbol{\Omega}\cdot\mathbf{U}$ in (2.12b) then delivers the expression ($\mathbf{I}$: identity)

$$\mathbf{b}(\boldsymbol{x},t)=\frac{h_0}{2}\mathbf{U}+\mathbf{B}(\mathbf{x},t)\mathbf{U}=[h_0/2\,\mathbf{I}+\mathbf{B}(\mathbf{x},t)]\mathbf{U} \quad (2.16)$$

where

$$[\mathbf{B}]=\begin{bmatrix}\left\langle\frac{h^3}{12\mu}\frac{\partial\Omega_1}{\partial y_1}\right\rangle & \left\langle\frac{h^3}{12\mu}\frac{\partial\Omega_2}{\partial y_1}\right\rangle\\ \left\langle\frac{h^3}{12\mu}\frac{\partial\Omega_1}{\partial y_2}\right\rangle & \left\langle\frac{h^3}{12\mu}\frac{\partial\Omega_2}{\partial y_2}\right\rangle\end{bmatrix}. \quad (2.17)$$

The advantage of the representation (2.16) is that it clearly reflects the sensitivity of the macroscopic flux $\mathbf{Q}$ to $\mathbf{U}$, $\partial\mathbf{Q}/\partial\mathbf{U}=h_0/2\,\mathbf{I}+\mathbf{B}$, which is important in a two-scale setting where $\mathbf{U}$ might be varying. Based on the treatment of the $\frac{\partial h}{\partial\tau}$ term in [15], it will now be shown that a similar conclusion can be reached for all lubrication regimes. Since the present form of the Reynolds equation is implicitly formulated with respect to an intermediate flat stationary plane, the following holds:

$$\frac{\partial h^{\pm}}{\partial\tau}=-\nabla_{\mathbf{y}}h^{\pm}\cdot\mathbf{U}^{\pm} \quad (2.18a)$$

Substitution of this expression into the right-hand side of (2.10c) by making use of (2.4) and rearranging delivers an alternative cell problem for w_3

$$\nabla_{\mathbf{y}}\cdot\left(\frac{h^3}{12\mu}\nabla_{\mathbf{y}}w_3\right)=-\frac{1}{2}\mathbf{V}\cdot\nabla_{\mathbf{y}}(h^+ + h^-) \quad (2.19a)$$

where $\mathbf{V}=\mathbf{U}^+-\mathbf{U}^-$. Hence, $w_3=-\boldsymbol{\Omega}(\mathbf{x},t,\mathbf{y},\tau)\cdot\mathbf{V}$ may be written in all lubrication regimes. Upon solving for Ω_1 and Ω_2, substitution of $w_3=-\boldsymbol{\Omega}\cdot\mathbf{V}$ in (2.12b) delivers the expression

$$\mathbf{b}(\boldsymbol{x},t,\tau)=\frac{h_0}{2}\mathbf{U}+\mathbf{B}(\mathbf{x},t,\tau)\mathbf{V} \quad (2.20)$$

where $\mathbf{B}$ still has the form (2.17). This result reflects the individual sensitivities of the macroscopic flux $\mathbf{Q}$ to $\mathbf{U}^+$ and $\mathbf{U}^-$: $\partial\mathbf{Q}/\partial\mathbf{U}^{\pm}=h_0/2\,\mathbf{I}\pm\mathbf{B}$. Since the first term in (2.20) does not depend on microscopic roughness, all microstructural influence that is associated with the motion of the surfaces is embedded in $\mathbf{B}$. Hence, for all regimes, the *homogenized coefficient tensors* $\mathbf{A}(\mathbf{x},t,\tau)$ and $\mathbf{B}(\mathbf{x},t,\tau)$ together reflect the microstructural influence onto the macroscale. For a homogeneous interface, $\mathbf{A}(\mathbf{x},t)=h_0^3/12\mu\,\mathbf{I}$ and $\mathbf{B}$ vanishes.

Scale transition theories based on a separation of scales assumption transfer the primal gradient and dual flux fields from the microscale to the macroscale through domain averaging. This is the link that is employed in a broad range of

works that address micromechanics and homogenization in the engineering literature. In such works, different boundary conditions are available for the microscopic (cell) problem and periodic boundary conditions are one of these. From this point of view, the application of the summarized approach to non-periodic microstructures essentially corresponds to averaging with periodic boundary conditions. The relation to the mathematical literature can be established by locally constructing a pseudo-periodic microstructure, the unit cell of which corresponds to a statistically representative sample. Once this construction is complete, the homogenization theory applies in its present form. The advantage of such a construction resides in the necessity of computing the (linearized) tangent operators, which are associated with $\boldsymbol{A}$ and $\boldsymbol{B}$ in the present work. The forms of these operators are directly implied by the homogenization framework but may be obscured when averaging is taken as the starting point. On the other hand, it is known that rapid local variations in a random microstructure may strongly affect the macroscale response and cause a failure of the scale separation assumption. Hence, periodicity is a more robust setting with respect to predictive capability.

2.3 Homogeneous-to-heterogeneous transitions

Clearly, $\mathbf{A}$ and $\mathbf{B}$, and hence p_0, rapidly oscillate with τ in the general unsteady case, which poses a computational difficulty since these oscillations must be resolved with a fine time discretization. To demonstrate the source of these oscillations, the unsteady 2D simple wedge problem (see Fig. 3) with microrough surfaces is solved in a coupled two-scale framework. Here both surfaces are periodically rough and the lower one is moving. The problem parameters are tabulated on Table 1. In all numerical investigations, the time and mesh resolutions are chosen to ensure a sufficiently converged numerical result.

The macroscopic pressure is monitored together with the corresponding microscopic interface in Fig. 4. The macroscopic pressure oscillates with the microscopic time τ. The maximum pressure is obtained if the peaks of the upper surface correspond to the peaks of the lower surface and similarly the valleys of the upper one match with the valleys of the lower one, i.e. when the macroscopic interface becomes heterogeneous (Fig. 4b) with the greatest root-mean-square (RMS) value of the film thickness. On the other hand, the minimum pressure is delivered if the peaks of the upper surface correspond to the valleys of the lower surface, i.e. when the microscopic interface becomes homogeneous (Fig. 4c) over the domain. This *homogeneous-to-heterogeneous transition* of the interface results in the oscillating macroscopic response with the microscopic time τ. In the quasi-stationary case, such a transition is not observed. The interface remains heterogeneous so that $\mathbf{A} = \mathbf{A}(\mathbf{x}, t)$ and $\mathbf{B} = \mathbf{B}(\mathbf{x}, t)$ such that the macroscopic response will not be a function of τ.

Table 1 The parameters of the 2D unsteady simple wedge problem (Fig. 4). Periodic microrough surfaces are employed in this example

Interface dimensions	mm × mm	$L_1 \times L_2$	1×1
Maximum mean film thickness	μm	h_{max}	1.5
Minimum mean film thickness	μm	h_{min}	0.5
Roughness root-mean-square	μm	RMS	0.2
Lower surface velocity	m/s	U^-	1
Lubricant (motor oil) viscosity	$Pa \cdot s$	μ	0.1

3 Time averaging

3.1 Eliminating fine-scale time dependence

Although the heterogeneous problem (2.1) is homogenized in space, the pressure in (2.11) is still oscillating with the microscale time (τ). The time average $(\cdot)^{\blacktriangledown} = \frac{1}{\Delta\tau}\int \cdot \, \mathrm{d}\tau$ of (2.11) is now taken in order to obtain a mean macroscopic response. A similar approach is applied to deliver the effective pressure in [48] where the time average of the heterogeneous Reynolds equation is taken. Presently, the proposed time-averaged macroscopic Reynolds equation is expressed as:

$$\nabla_{\mathbf{x}} \cdot \left(\mathbf{A}^{\blacktriangledown}(\mathbf{x}, t)\nabla_x p_0'(\mathbf{x}, t)\right) = \nabla_{\mathbf{x}} \cdot \mathbf{b}^{\blacktriangledown}(\mathbf{x}, t) + \frac{\partial h_0}{\partial t}. \tag{3.1}$$

Here, the right-hand side corresponds to the time average of the right-hand-side of (2.11)

$$\left[\nabla_{\mathbf{x}} \cdot \mathbf{b}(\mathbf{x}, t, \tau) + \frac{\partial h_0}{\partial t}\right]^{\blacktriangledown} = \nabla_{\mathbf{x}} \cdot \mathbf{b}^{\blacktriangledown}(\mathbf{x}, t) + \frac{\partial h_0}{\partial t} \tag{3.2}$$

while the left-hand side approximates the time average of the left-hand-side of (2.11)

$$[\nabla_{\mathbf{x}} \cdot (\mathbf{A}(\mathbf{x}, t, \tau)\mathbf{G}(\mathbf{x}, t, \tau))]^{\blacktriangledown} \approx \nabla_{\mathbf{x}} \cdot \left(\mathbf{A}^{\blacktriangledown}(\mathbf{x}, t)\nabla_{\mathbf{x}} p_0'(\mathbf{x}, t)\right) \tag{3.3}$$

where the macroscopic pressure gradient has been represented as $\mathbf{G} = \langle \mathbf{g} \rangle = \nabla_{\mathbf{x}} p_0$. This approximation is investigated by splitting the terms into mean $(\cdot)^{\blacktriangledown}$ and oscillatory $\tilde{(\cdot)}$ parts:

$$\mathbf{A}(\mathbf{x}, t, \tau) = \mathbf{A}^{\blacktriangledown}(\mathbf{x}, t) + \tilde{\mathbf{A}}(\mathbf{x}, t, \tau), \tag{3.4a}$$

$$\mathbf{G}(\mathbf{x}, t, \tau) = \mathbf{G}^{\blacktriangledown}(\mathbf{x}, t) + \tilde{\mathbf{G}}(\mathbf{x}, t, \tau). \tag{3.4b}$$

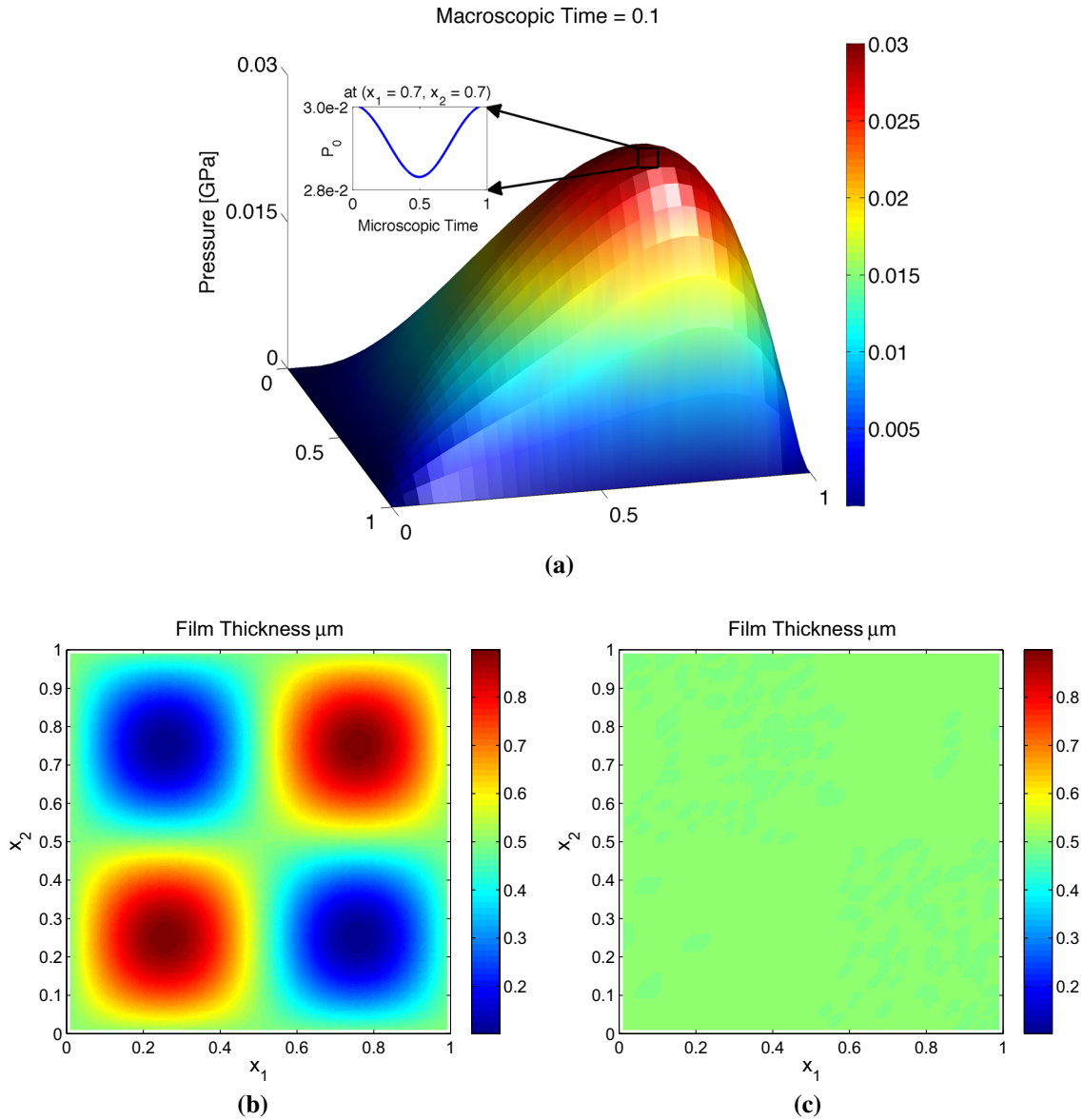

Fig. 4 The unsteady 2D wedge problem is solved. The oscillation of the homogenized pressure distribution (shown at the instant of a heterogeneous film) is monitored at the point where the pressure is a maximum. The results demonstrate that the heterogeneous-to-homogeneous transition of the interface is the source of the macroscopic pressure oscillation with the microscopic time τ. The amplitude of these oscillations will depend on the variation of the local film thickness, which is influenced by the mean film thickness and the surface roughness. **a** $\tau = \tau_i$: homogenized pressure. **b** $\tau = \tau_i$: heterogeneous film. **c** $\tau = \tau_i + \Delta\tau$: homogeneous film

Based on the expressions above, (3.3) is equivalent to

$$\begin{aligned}[\nabla_{\mathbf{x}} \cdot (\mathbf{AG})]^{\blacktriangledown} &= \nabla_{\mathbf{x}} \cdot [(\mathbf{A}^{\blacktriangledown} + \tilde{\mathbf{A}})(\mathbf{G}^{\blacktriangledown} + \tilde{\mathbf{G}})]^{\blacktriangledown} \\ &= \nabla_{\mathbf{x}} \cdot (\mathbf{A}^{\blacktriangledown}\mathbf{G}^{\blacktriangledown} + \mathbf{A}^{\blacktriangledown}\tilde{\mathbf{G}}^{\blacktriangledown} + \tilde{\mathbf{A}}^{\blacktriangledown}\mathbf{G}^{\blacktriangledown} + (\tilde{\mathbf{A}}\tilde{\mathbf{G}})^{\blacktriangledown}) \\ &= \nabla_{\mathbf{x}} \cdot (\mathbf{A}^{\blacktriangledown}\mathbf{G}^{\blacktriangledown} + (\tilde{\mathbf{A}}\tilde{\mathbf{G}})^{\blacktriangledown}) \\ &\approx \nabla_{\mathbf{x}} \cdot \left(\mathbf{A}^{\blacktriangledown}\nabla_{\mathbf{x}} p_0'\right). \end{aligned} \tag{3.5}$$

Since $\mathbf{G}^{\blacktriangledown} = \nabla_{\mathbf{x}} p_0^{\blacktriangledown}$, the proposed time averaging method approximates the mean homogenized pressure satisfactorily, i.e. $p_0' \approx p_0^{\blacktriangledown}$, as long as the term $\tilde{\mathbf{A}}\tilde{\mathbf{G}}$ is small or its time average is of negligible magnitude, which is to be demonstrated next. In general, one might postulate that there is a (non-dimensional) factor associated with the ratio of a measure of roughness to the mean film thickness ratio which controls the magnitude of this neglected contribution. One might even attempt to model this dependence, perhaps not too unlike how one models the Reynolds stress in turbulence. Such an approach goes beyond the scope of this work and will not be pursued.

Both for periodic and random surfaces, the duration $\Delta\tau$ of averaging corresponds to the time it takes for one sam-

Table 2 The parameters of the 1D unsteady simple wedge problem are listed

Interface length	mm	L	1
Maximum mean film thickness	μm	h_{max}	1.5
Minimum mean film thickness	μm	h_{min}	0.5
Roughness wavelength for deterministic solution	mm	ε	0.02
Lower surface velocity	m/s	U^-	1
Lubricant viscosity	$Pa{\cdot}s$	μ	0.05

ple to fully traverse the span of the other. For commensurate periodicity (Sect. 3.2), $\Delta\tau$ truly corresponds to a period $\mathcal{T}$ of the oscillations. For incommensurate periodicity and randomness, the unit cell is associated with a pseudo-periodic microstructure construction and once this construction is made $\Delta\tau$ again delivers a period of the oscillations.

3.2 Periodic roughness

In order to observe the macroscopic response in the unsteady case with periodic microrough surfaces and judge the efficacy of the proposed time averaging, the 1D two-scale wedge problem is considered. Both surfaces are rough and only the lower one is moving. The mean film thickness is expressed as $h_0 = h_{max} - \frac{h_{max}-h_{min}}{L} x_1$ (see Fig. 3). The problem parameters are listed on Table 2. Additionally, the roughness RMS is initially set to 0.1 μm. In Fig. 5, the time-averaged deterministic pressure ($p_\varepsilon^{\blacktriangledown}$) is compared with the time-averaged homogenized pressure ($p_0^{\blacktriangledown}$) and the solution to the time-averaged homogenized equation (p_0'). The macroscopic pressure distribution oscillates between a maximum (p_ε^{max}) and a minimum (p_ε^{min}). The time-averaged homogenized pressure ($p_0^{\blacktriangledown}$) already captures the time-averaged deterministic pressure ($p_\varepsilon^{\blacktriangledown}$) even though the roughness wavelength is far from satisfying the homogenization assumption $\varepsilon \to 0$. Additionally, the proposed time averaging method delivers a solution p_0' which can accurately capture $p_0^{\blacktriangledown}$ for low roughness RMS (see Fig. 5a). When the roughness RMS increases (see Fig. 5b), p_ε^{max} increases while p_ε^{min} does not change, due to the fact that the mean film thickness variation is the same for both problems and the minimum pressure distribution is associated with this variation. In this case, the proposed time averaging method is not able to predict $p_0^{\blacktriangledown}$ accurately. Nevertheless, it can be considered as a reasonable first-order estimation for the mean response which is easy to compute due to the absence of the fine-scale time τ.

So far, commensurate periodic surfaces as in Fig. 6a-1 have been studied. However, periodic surfaces might also be incommensurate (see [49]), i.e. the ratio of the frequencies of the roughness on two surfaces can be an irrational number, see Fig. 6b-1. Using the parameters on Table 2, the unsteady 1D wedge problem is solved deterministically with incommensurate surfaces having a roughness RMS of 0.1 μm and the results are summarized in Fig. 7. The roughness frequency (f) of the upper surface is set to three different values (i.e. $[f_1^+, f_2^+, f_3^+] = [15\sqrt{2}, 60\sqrt{2}, 300\sqrt{2}]$) while the lower surface has the corresponding roughness frequencies of $[f_1^-, f_2^-, f_3^-] = [15, 60, 300]$. In these cases, p_ε still oscillates with time between p_ε^{max} and p_ε^{min}. However, the oscillations are smaller than the commensurate case (see Fig. 5a) despite having the same roughness RMS. Additionally, Fig. 7c demonstrates that the oscillation with time vanishes as the frequency of the roughness increases (i.e. with increasing sample size). In other words, when the surfaces are incommensurate the macroscopic response is independent of the microscopic time even in the unsteady case, which is a con-

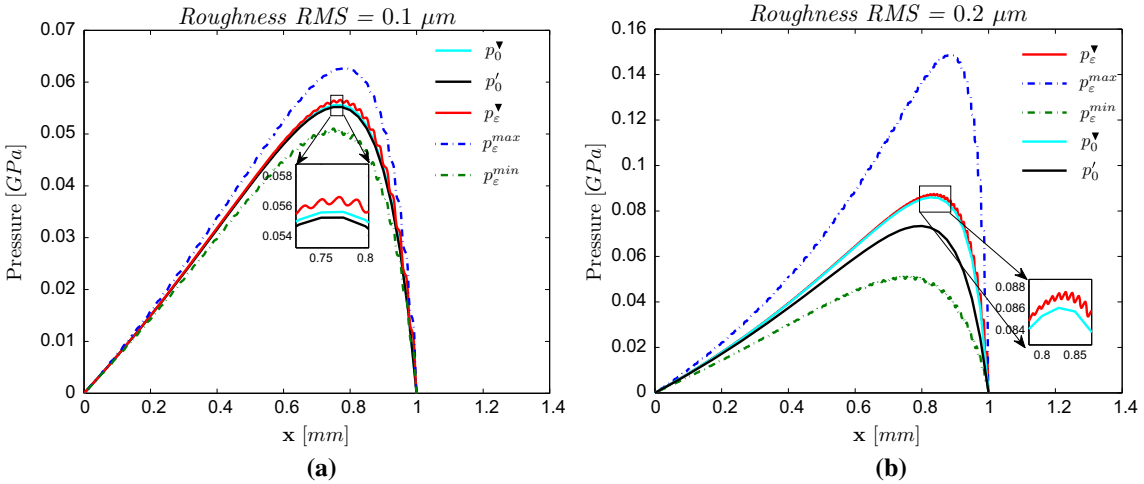

Fig. 5 The unsteady 1D wedge problem with periodic microrough surfaces is solved and the efficacy of the proposed time averaging method is demonstrated in both cases of low roughness RMS (**a**) and high roughness RMS (**b**). **a** Low RMS. **b** High RMS

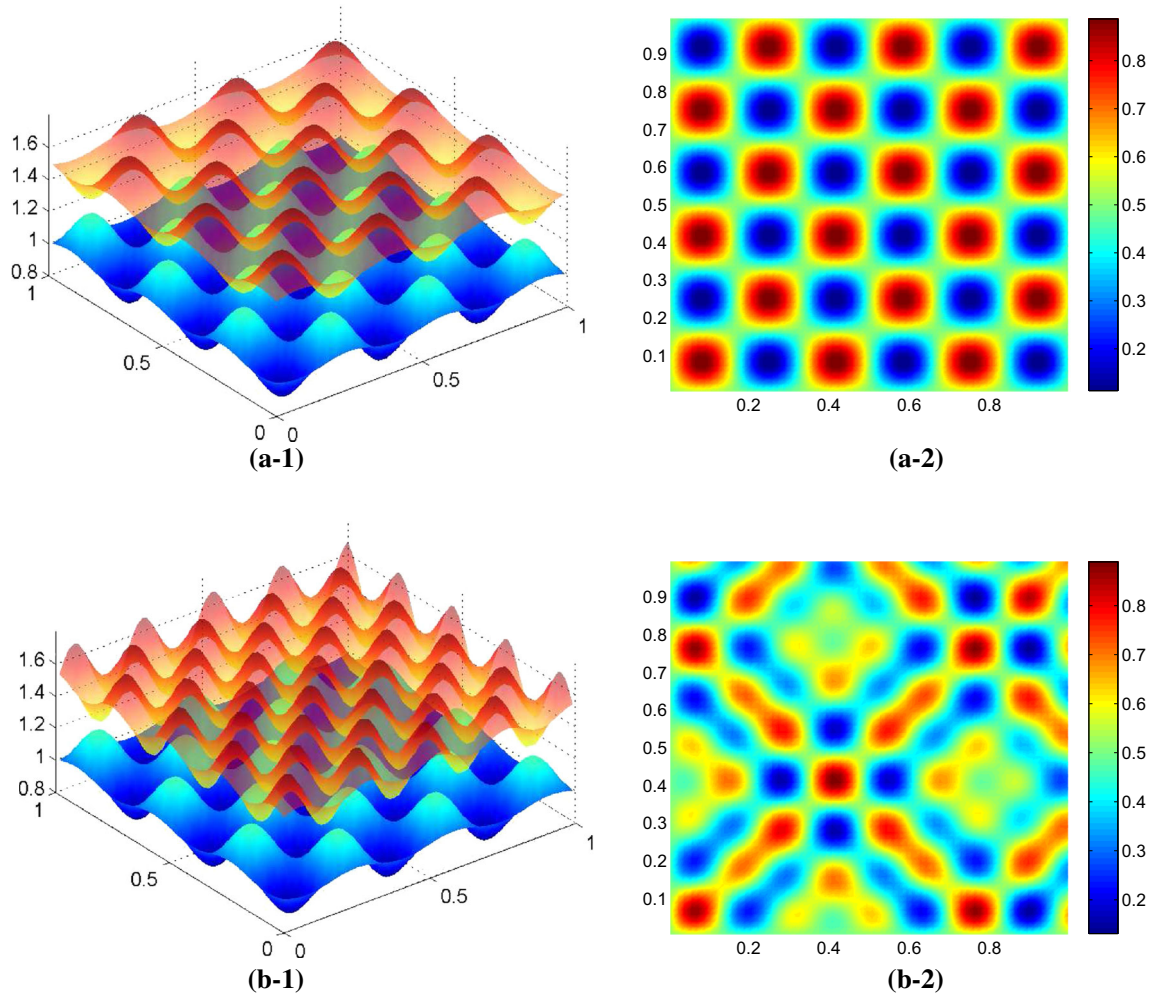

Fig. 6 Commensurate (**a-1**) and incommensurate (**b-1**) surfaces are depicted with corresponding film thicknesses (**a-2**) and (**b-2**). The *upper* and *lower* surfaces match in the commensurate case, which leads to periodic film thickness during the motion unlike the incommensurate ones which delivers a non-periodic film thickness. Note that the translation of one periodic surface with respect to the other one will simply introduce a phase-shift in the microscopic pressure-time profile and hence does not require an independent investigation. **a-1** Commensurate surfaces. **a-2** Commensurate h distribution. **b-1** Incommensurate surfaces. **b-2** Incommensurate h distribution

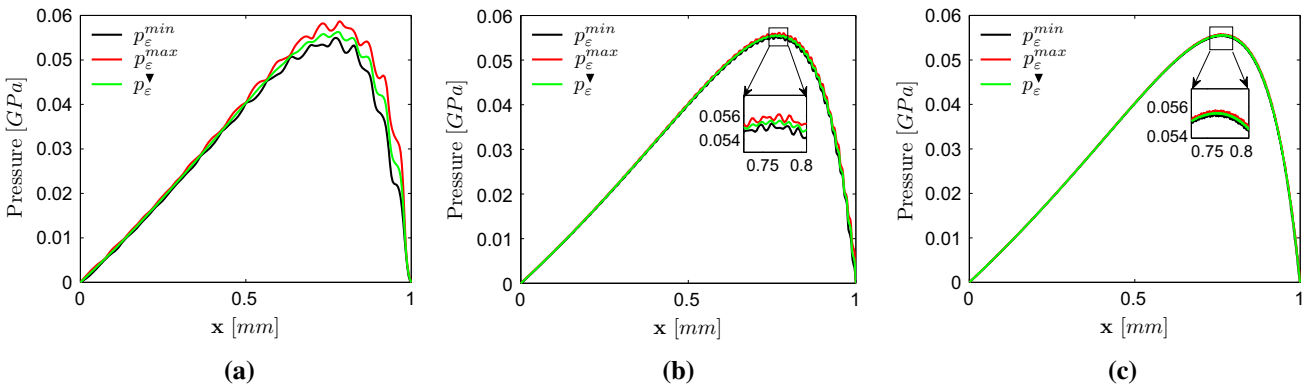

Fig. 7 Despite the use of the periodically rough surfaces, oscillations with time vanish in the case of incommensurate surfaces. **a** $f_1^+ = 15\sqrt{2}$, $f_1^- = 15$. **b** $f_2^+ = 60\sqrt{2}$, $f_1^- = 60$. **c** $f_3^+ = 300\sqrt{2}$, $f_1^- = 300$

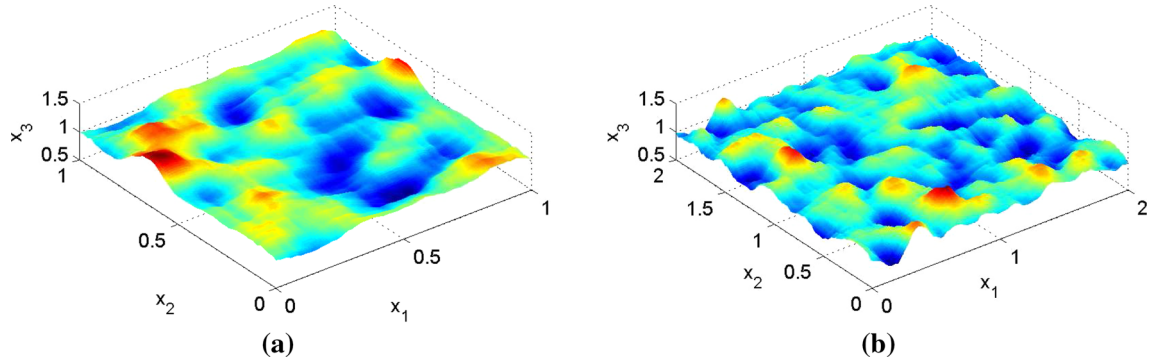

Fig. 8 The random surfaces are generated using the RFM with a correlation length of 5 pixels. 50 × 50 pixel space is mapped onto a FEM mesh with 50 × 50 elements and similarly 100 × 100 pixel space is mapped onto a mesh with 100 × 100 elements. **a** Small sample size generated from 50 × 50 pixel space. **b** Large sample size generated from 100 × 100 pixel space

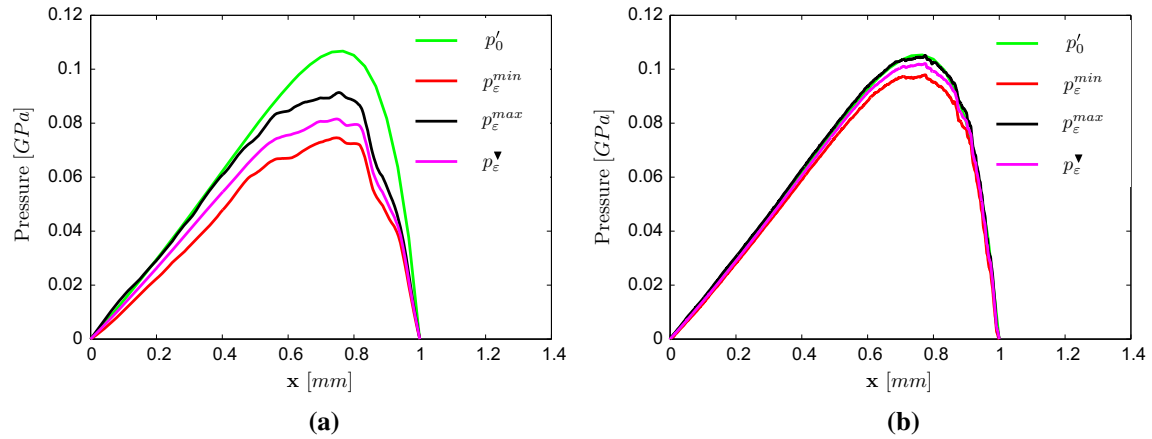

Fig. 9 The unsteady wedge problem is solved in 1D with 1D random microrough surfaces that are generated through the algorithm demonstrated in Fig. 8. Note that the sample size effect on the macroscopic response is similar to the case of periodic incommensurate rough surfaces (Fig. 7). **a** Small sample size. **b** Large sample size

venient simplification of the original theoretical implication. An important consequence of this observation is that since random microrough surfaces are generally incommensurate as well, the macroscopic response is expected not to oscillate with the microscopic time in the unsteady case with such surfaces. This will be verified in the following section.

3.3 Random roughness

Real surfaces are inherently randomly rough. In order to understand the time-dependent lubrication phenomenon for such surfaces, isotropic random roughness is generated through the random-field model (RFM) which is an algorithm to generate Gaussian surfaces from a set of random variables (see [50–52]). For this purpose, a pixel space digitized into $N \times N$ pixels is taken and a random film thickness value generated by a Gaussian random number generator is assigned to each pixel. Then the random field is smoothed with a filter having a Gaussian kernel and a correlation length measured with the number of pixels for fixed pixel length, which controls the roughness wavelength and is chosen to be 5 pixels in this study. The generated surface is then mapped onto a FEM mesh through a least squares procedure wherein periodicity conditions are imposed to obtain matching roughness profiles on opposing edges, which is necessary for the applicability of the homogenization theory (see Sect. 2.2). The imposition of periodicity modifies the nature of randomness, however this modification is restricted to regions near the boundaries of the sample and hence its influence diminishes with increasing sample size. The RFM delivers sample random surfaces which are depicted on Fig. 8 for small and large sample sizes.

The macroscopic response and the proposed time averaging method is first tested with random microrough surfaces by solving the unsteady 1D wedge problem (see Fig. 3) with the parameters tabulated on Table 2 with an RMS of 0.1 μm and $\mu = 0.1\ Pa \cdot s$. The results (Fig. 9) resemble the ones delivered by the periodic incommensurate surfaces (Fig. 7) and clearly suggest that the macroscopic response is not a function of the microscopic time for sufficiently large sample

Table 3 The parameters of the stationary 2D microscopic problem for the initial random sample are listed

Interface dimensions	mm	$L \times L$	1×1
Mean film thickness	μm	h_0	1
Roughness root-mean-square	μm	RMS	0.2
Lubricant viscosity	$Pa \cdot s$	μ	0.14
Macroscopic pressure gradient	Pa/mm	$\nabla_{\mathbf{x}} p_0$	$[1\ 0]$
Initial Pixel space		$N \times N$	10×10
Initial FEM mesh size		$E \times E$	10×10

sizes. Additionally, it is again observed that the deterministic solution rapidly approaches the homogenization prediction with increasing roughness frequency from Fig. 9a, b. In other words, $\mathbf{A}(\mathbf{x}, t, \tau) \approx \mathbf{A}(\mathbf{x}, t)$, $\mathbf{B}(\mathbf{x}, t, \tau) \approx \mathbf{B}(\mathbf{x}, t)$ and hence $p_0(\mathbf{x}, t, \tau) \approx p_0(\mathbf{x}, t)$. As a result, with increasing sample size, $p_\varepsilon^{\blacktriangledown}$ also approaches to p_0' which is computed by using a 50×50 sample at the microscale. The effect of this chosen microscale sample size on the homogenization results is investigated next.

For the periodic microstructure, the representative interface element is the unit cell of the structure. However, if the medium is random, the representative element is the set of microstructural elements displaying the statistical and the spectral properties of the macrostructure. See [51,53,54] for further details on random microstructures. In practice, a representative element is determined through sample enlargement in combination with ensemble averaging, indicated by $\langle\langle\cdot\rangle\rangle$. To illustrate this, the 2D microscopic problem is studied with nominally flat isotropic random microrough surfaces. The problem parameters are listed on Table 3. The sample size is controlled by the pixel dimension N with a proportional increase in the interface dimensions L and the FEM mesh size E. The eigenvalues of the homogenized coefficient tensors $\mathbf{A}$ and $\mathbf{B}$ are monitored in Fig. 10 in order to check the convergence in the predicted macroscopic response with increasing sample size. Here, the error bars show the standard deviation of the eigenvalues for a given sample size while a solid line tracks the ensemble average $\langle\langle\lambda\rangle\rangle$ of an eigenvalue. There are 400 samples for the sample sizes of $N = \{10, 20, 40, 70, 80\}$, 200 samples for the sample size of $N = 100$, and 100 samples for the sample size of $N = 200$. Clearly, ensemble averaging together with sample enlargement alleviates randomness effects on the macroscopic response and delivers the effective macroscopic response.

The setting discussed above for the determination of the sample size applies to both the stationary and the quasi-stationary cases where only one surface has random roughness. In the unsteady case where both surfaces are rough, the additional factor of microscopic time τ must be considered. Although the macroscopic response has been observed not to be a function of τ in the unsteady case with an appropriately large sample, one might now ask whether the proposed time averaging method still has an advantage. Specifically, can time averaging accelerate the convergence in ensemble averaging for the determination of the appropriate sample size? This question is addressed by studying the unsteady 2D microscopic problem with nominally flat surfaces for which the parameters are listed on Table 4. By increasing the sample size, the convergence of the ensemble-time-averaged macroscopic response (in this case the fluid flux $\langle\langle\mathbf{Q}^{\blacktriangledown}\rangle\rangle$) is summarized in Fig. 11a. The number of samples (s) for different sample sizes $N = \{10, 20, 30, 40, 50, 60, 70, 80, 90, 120\}$ is chosen as $s = \{50, 45, 40, 35, 30, 25, 20, 15, 10, 10\}$. The ensemble average of the time-averaged macroscopic response is taken for each sample size and $\langle\langle\mathbf{Q}^{\blacktriangledown}\rangle\rangle$ is plotted in Fig. 11b. On the other hand, one can also monitor the ensemble average

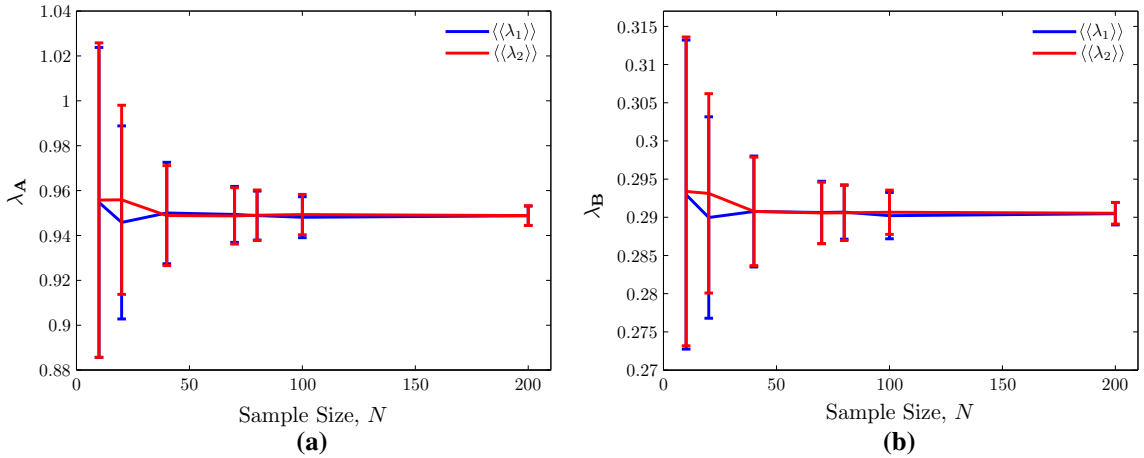

Fig. 10 The sample enlargement and the ensemble averaging, together, deliver the effective macroscopic response with identical eigenvalues due to isotropy. Although the observations apply to both the stationary and the quasi-stationary cases, the calculations of the eigenvalues assumes the stationary case. **a** Eigenvalues of coefficient tensor **A**. **b** Eigenvalues of coefficient tensor **B**

Table 4 The parameters of the unsteady 2D microscopic problem with a random sample of the smallest sample are listed

Interface dimensions	mm	$L \times L$	1×1
Mean film thickness	μm	h_0	1
Roughness root-mean-square	μm	RMS	0.1
Lubricant viscosity	$Pa \cdot s$	μ	0.1
Velocity of the lower surface	m/s	$\mathbf{U}^-$	10
Macroscopic pressure gradient	Pa/mm	$\nabla_{\mathbf{x}} p_0$	$[1\ 0]$
Initial Pixel space		$N \times N$	10×10
Initial FEM mesh size		$E \times E$	10×10

$\langle\langle \mathbf{Q} \rangle\rangle$ of responses measured at fixed observation times τ. Fig. 11b shows that this is a very good approximation of $\langle\langle \mathbf{Q}^{\blacktriangledown} \rangle\rangle$. Therefore, one can conclude that ensemble averaging renders time averaging statistically unnecessary (but not vice versa). The practical implication of this is that the unsteady 2D problem with random microrough surfaces can be considered as quasi-stationary on the microscale, which significantly eases the computational burden. In other words, it is sufficient to calculate **A** and **B** *only* for a chosen starting configuration for each sample and subsequently carry out ensemble averaging together with sample enlargement in order to determine an appropriate microscopic sample size.

4 Surface deformation

4.1 Taylor assumption

In the case of soft elastohydrodynamic lubrication, one might consider solving a coupled deformation - lubrication problem on the microscale (see [10,40,55,56]). In [40], within a scale separation assumption, the coupled microscopic problem was condensed to a decoupled two-phase micromechanical test where (i) the macroscopic surface deformation is imposed on the micromechanical sample together with the macroscopic pressure on the rough surface, and subsequently (ii) the microscopic lubrication problem is solved on a frozen texture that is extracted from the deformed sample in order to determine the macroscopic homogenized interface response. Since the application of the pressure does not alter the roughness characteristics, the macroscopic surface deformation remains as the only macroscopic variable in the first phase. In the present study, as an alternative to reflecting its effect through FEM analysis, a uniform projection into the cell will be pursued. This corresponds to the numerically efficient Taylor assumption

$$\mathbf{x} = \mathbf{F}_s \mathbf{X} \tag{4.1}$$

where $\mathbf{x}$ and $\mathbf{X}$ are the position vectors on the deformed and undeformed surfaces respectively, and $\mathbf{F}_s$ is the macroscopic surface deformation gradient which is denoted in component form as

$$[\mathbf{F}_s] = \begin{bmatrix} f_{11} & f_{12} \\ f_{21} & f_{22} \end{bmatrix}. \tag{4.2}$$

It has already been shown that the unsteady case with random or incommensurate periodic microrough surfaces condenses to the quasi-stationary case, which also represents a generalization of the stationary case. Therefore, without loss of generality, the quasi-stationary case will be considered, based on the parameters listed on Table 5. Initially, a periodic microrough surface is assumed in order to concentrate on the main features of deformation effects and subsequently randomness is incorporated.

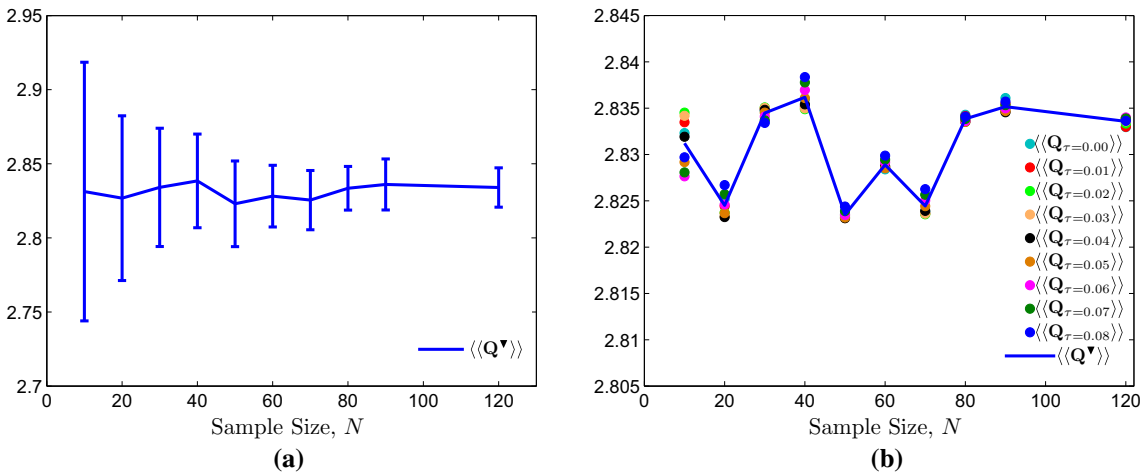

Fig. 11 The limit delivered by combined ensemble averaging and sample enlargement in the unsteady case is depicted on (**a**) for the time-averaged macroscopic response. On the other hand, **b** indicates that monitoring the ensemble averaged response at fixed observation times τ is sufficient. **a** Time-averaged macroscopic response. **b** $\langle\langle \mathbf{Q} \rangle\rangle$ at various time steps

Table 5 The parameters of the quasi-stationary 2D microscopic problem with a periodic microrough deformable surface

Interface dimensions	mm	$L \times L$	0.5×0.5
Mean film thickness	μm	h_0	0.5
Roughness root-mean-square	μm	RMS	0.2
Roughness wavelength on undeformed surface	mm	ε	0.25
Lubricant viscosity	$Pa \cdot s$	μ	0.14
Velocity of the lower surface	m/s	$\mathbf{U}^-$	1

4.2 Area-preserving deformations

The surfaces are either (i) sheared using $f_{12} = \{0.2, 0.4, 0.6\}$, or (ii) stretched using $f_{11} = \{1.2, 1.4, 1.6\}$ with corresponding $f_{22} = \{\frac{1}{1.2}, \frac{1}{1.4}, \frac{1}{1.6}\}$. Thus, both deformations are macroscopically area-preserving: $\det \mathbf{F}_s = 1$. The deformed surfaces are shown on Fig. 12. Here, the first row shows the deformed configurations delivered by solving the deformation within a FEM framework using periodic boundary conditions on a boundary layer sample with a rough surface and subsequently extracting the deformed surface topography. The figures in the second row are the results of the Taylor assumption. In order to compare the macroscopic response of these two sets of surfaces, the magnitude of **AG** is plotted on Fig. 13 where $\{\mathbf{G}\} = \{cos(\theta)\ sin(\theta)\}^T$ for $\theta = 0...2\pi$. The initial response of the periodic cell is isotropic and deformation induces an anisotropic response. Clearly, the Taylor assumption is able to capture both the magnitude and the direction of this deformation-induced anisotropy satisfactorily. Although there is a small mismatch at large deformations, the negligible cost of the Taylor assumption in comparison to the high cost of a microscale FEM analysis of surface deformation significantly outweighs this disadvantage. From this point of view, the Taylor assumption may be viewed as an enabling approach towards the two-scale computational homogenization analysis of lubricated soft microrough interfaces where the response of a macroscopically deforming interface is obtained through the coupled solution of microscopic soft elastohydrodynamic problems.

The comparison was also carried out with different combinations of material parameters (bulk and shear moduli) as well as for different isotropic hyperelastic material models (Ogden and Neo-Hooke). Results (not shown) indicate that the quality of approximation is retained, which is advantageous since the Taylor assumption is insensitive to the choice of the material. The quality is also retained when the area-preserving shear and stretch deformations are combined as

$$[\mathbf{F}_s^1] = \begin{bmatrix} 1+\phi & \phi \\ 0 & \frac{1}{1+\phi} \end{bmatrix} \tag{4.3}$$

the results of which are summarized in Fig. 14. Here, one also observes that when the material approaches an incompressible response ($\nu = 0.5$) that is typically observed for soft polymeric materials, the prediction capability increases further. In the remaining examples, near incompressibility ($\nu = 0.495$) will be assumed. In all cases, the error remains small in comparison with the large deviations from the undeformed (isotropic) response. This is also verified with a different combined shear-stretch area-preserving deformation:

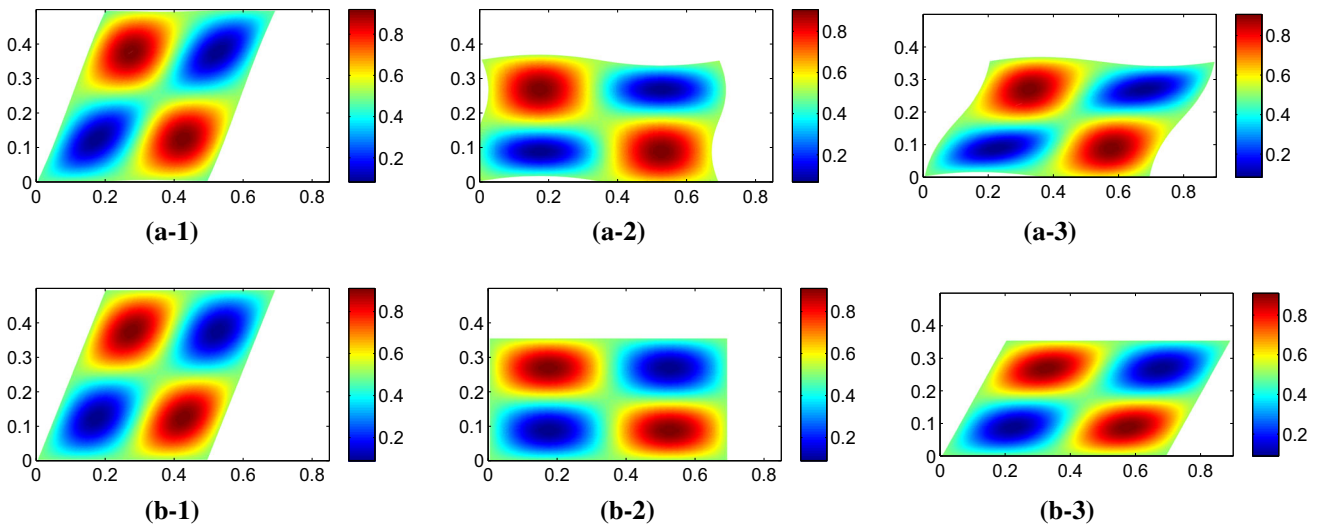

Fig. 12 Effect of macroscopic surface deformation on the sample configuration is depicted, together with the film thickness distribution. The first row shows the deformed configurations delivered by FEM with a Poisson's ratio of $\nu = 0.385$ and the second row is obtained through the Taylor assumption. **a-1** Shear = 0.4. **a-2** Tension = 1.4. **a-3** Shear = 0.4, Tension = 1.4. **b-1** Shear = 0.4. **b-2** Tension = 1.4. **b-3** Shear = 0.4, Tension = 1.4

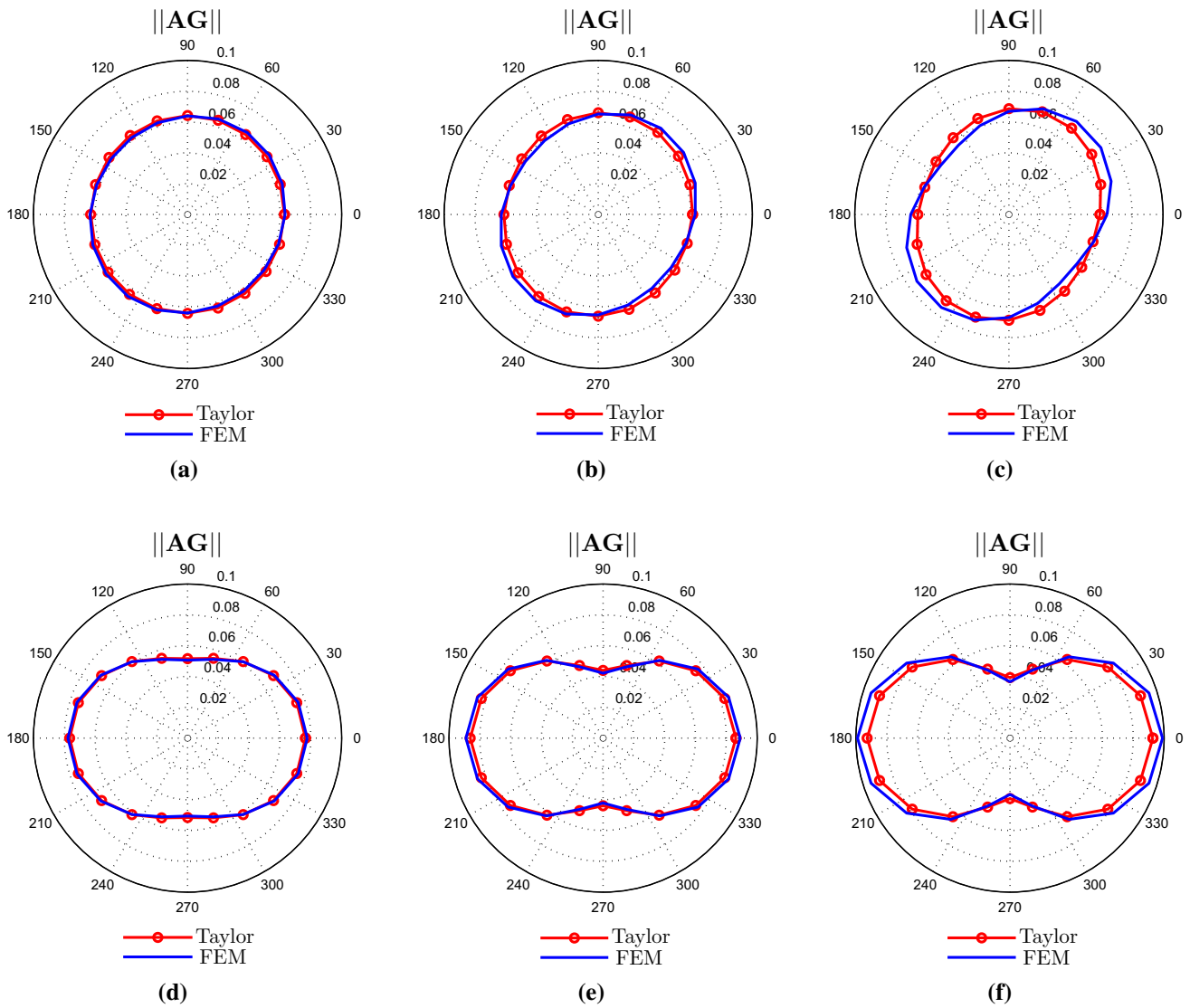

Fig. 13 The polar plots of the magnitudes of **AG** for the area-preserving deformation types (shear and tension) incorporated into the problem with two different ways (the Taylor assumption and the FEM framework) are depicted. Here, Poisson's ratio ν is set to 0.385. **a** Shear = 0.2, **b** Shear = 0.4, **c** Shear = 0.6, **d** Tension = 1.2, **e** Tension = 1.4, **f** Tension = 1.6

$$[\mathbf{F}_s^2] = \begin{bmatrix} 1+\phi & \phi \\ -\phi & 1-\phi \end{bmatrix} \tag{4.4}$$

The results in Fig. 15 reinforce the conclusion that the Taylor assumption can replace the FEM approach in reflecting area-preserving deformations onto the microscopic problem both qualitatively and quantitatively. Similar observations hold for **B** as summarized in Fig. 16 where $\{\mathbf{V}\} = \{cos(\theta)\ sin(\theta)\}^T$.

4.3 Non-area-preserving deformations

Although the Taylor assumption is highly predictive for area-preserving deformations, it has shortcomings that reflect on non-area-preserving deformations ($\det \mathbf{F}_s \neq 1$). For instance, it preserves all out-of-plane statistical characteristics, i.e. the central moments of the roughness. Consequently, deviations from the FEM predictions can be anticipated. This is tested by perturbing the combined shear-stretch area-preserving deformation gradients (4.3) and (4.4) evaluated at $\phi = 0.4$:

$$[\mathbf{F}_s^{1,\gamma}] = \begin{bmatrix} 1.4+\gamma & 0.4 \\ 0 & \frac{1}{1.4} \end{bmatrix}, \quad [\mathbf{F}_s^{2,\gamma}] = \begin{bmatrix} 1.4 & 0.4+\gamma \\ -0.4 & 0.6 \end{bmatrix}. \tag{4.5}$$

Here, γ controls the degree to which the deformation is non-area-preserving. The results in Figures 17 and 18 show

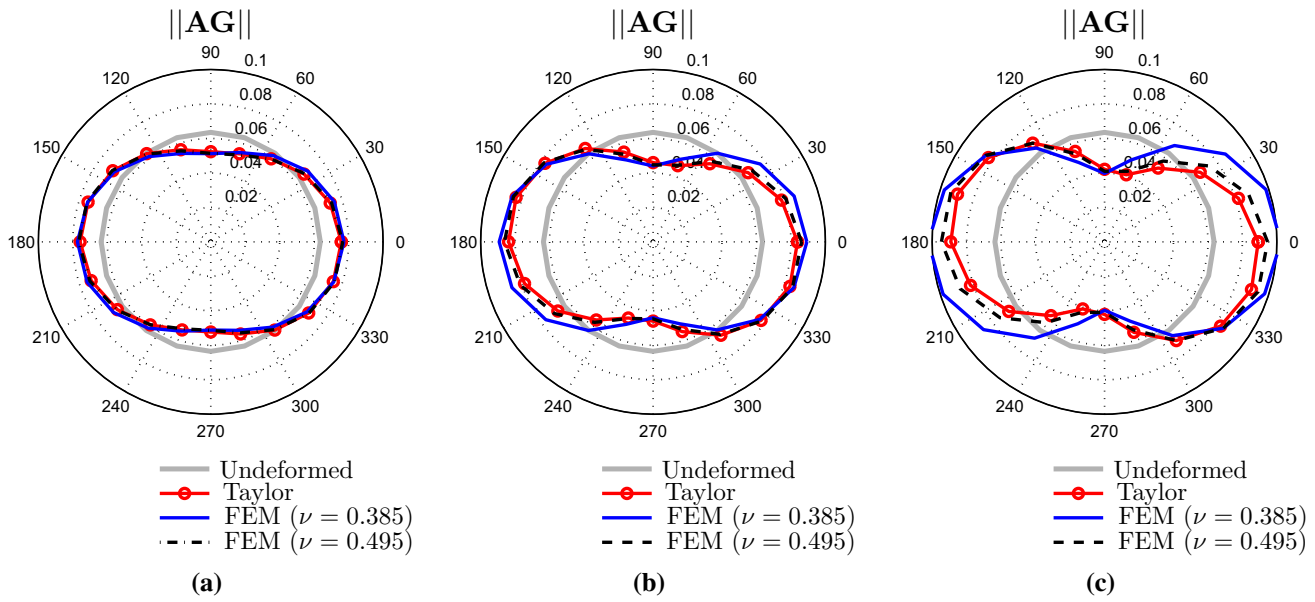

Fig. 14 The macroscopic responses are depicted for shear-stretched combined area-preserving deformation (4.3) are depicted. The response of the undeformed sample is isotropic, which is indicated in this and all following figures. Additionally, the effect of Poisson's ratio (ν) is illustrated by choosing a compressible material with $\nu = 0.385$ and a nearly-incompressible material with $\nu = 0.495$. **a** $\mathbf{F}_s^1$ with $\phi = 0.2$, **b** $\mathbf{F}_s^1$ with $\phi = 0.4$, **c** $\mathbf{F}_s^1$ with $\phi = 0.6$

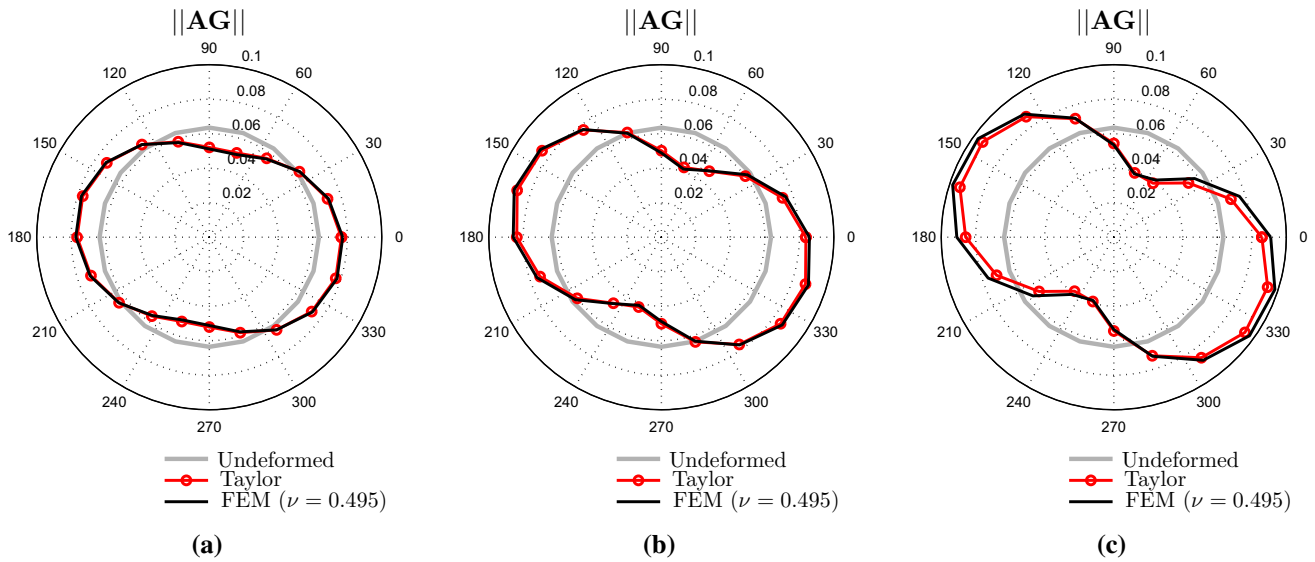

Fig. 15 The macroscopic responses are depicted for shear-stretch combined deformations with the deformation gradient (4.4). **a** $\mathbf{F}_s^2$ with $\phi = 0.2$, **b** $\mathbf{F}_s^2$ with $\phi = 0.4$, **c** $\mathbf{F}_s^2$ with $\phi = 0.6$

that the deformation-induced anisotropy is qualitatively still captured well. For a decreasing area, i.e. when $\det \mathbf{F}_s < 1$ ($\gamma < 0$), the Taylor assumption delivers quantitative deviations with both types of deformation gradients for **A** (see Fig. 17a-1, b-1) and **B** (see Fig. 18a-1, b-1). On the other hand, increasing area, i.e. $\det \mathbf{F}_s > 1$ ($\gamma > 0$), may (Fig. 17a-2, a-3 for **A**, Fig. 18b-2, b-3 for **B**) or may not (Fig. 17b-2, b-3 for **A**, 18a-2, a-3 for **B**) lead to quantitative deviations. In all cases, a good agreement is observed for moderate values of $\det \mathbf{F}_s > 1$ and the nature of anisotropy is captured well even at large values. It should also be noted that $\det \mathbf{F}_s$ cannot be much smaller than 1. For instance, the lubrication theory ceases to be valid when γ is further decreased from -0.29 to -0.3 in Fig. 17b-1 because contact is initiated among the two surfaces. Consequently, the deviations observed are bounded. Studies towards the improvement of the Taylor assump-

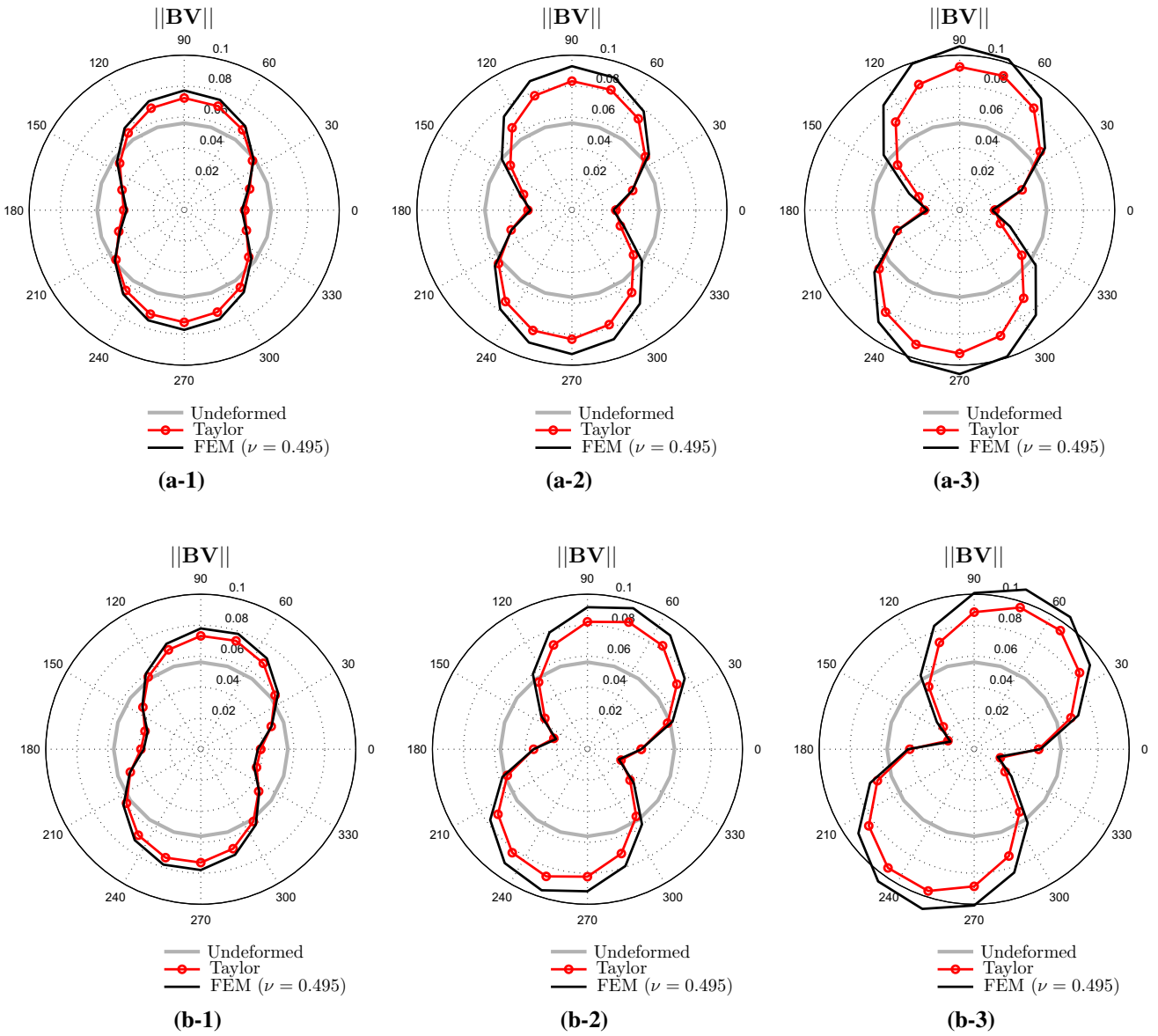

Fig. 16 The macroscopic responses (i.e. the homogenized coefficient tensor **B** in this case) are depicted for shear-stretch combined area-preserving deformations with the gradients (4.3) (*upper row*) and (4.4) (*lower row*). **a-1** $\mathbf{F}_s^1$ with $\phi = 0.2$, **a-2** $\mathbf{F}_s^1$ with $\phi = 0.4$, **a-3** $\mathbf{F}_s^1$ with $\phi = 0.6$, **b-1** $\mathbf{F}_s^2$ with $\phi = 0.2$, **b-2** $\mathbf{F}_s^2$ with $\phi = 0.4$, **b-3** $\mathbf{F}_s^2$ with $\phi = 0.6$

tion at significantly large deformations is planned as future work.

4.4 Randomness

To demonstrate the advantage of the Taylor assumption, a series of random roughness cases is studied where the large sample sizes would lead to significant FEM costs. Here, the particular case of combined shear-stretch area-preserving deformation gradient $\mathbf{F}_s^{2,\gamma}$ in (4.5) is considered with $\gamma = 0.3$. Using the Taylor assumption, this deformation is applied to random microrough surfaces which are generated as in Section 3.3. The problem parameters correspond to those on Table 5 but the mean film thickness is increased to 0.6 μm to avoid contact initiation among the surfaces during deformation.

The results are summarized in Fig. 19. For each sample size, the macroscopic responses of three different samples are plotted together for the deformed and undeformed configurations. Small samples display anisotropy even when they are undeformed, the magnitude and direction of which additionally depends on the particular sample, despite the isotropic

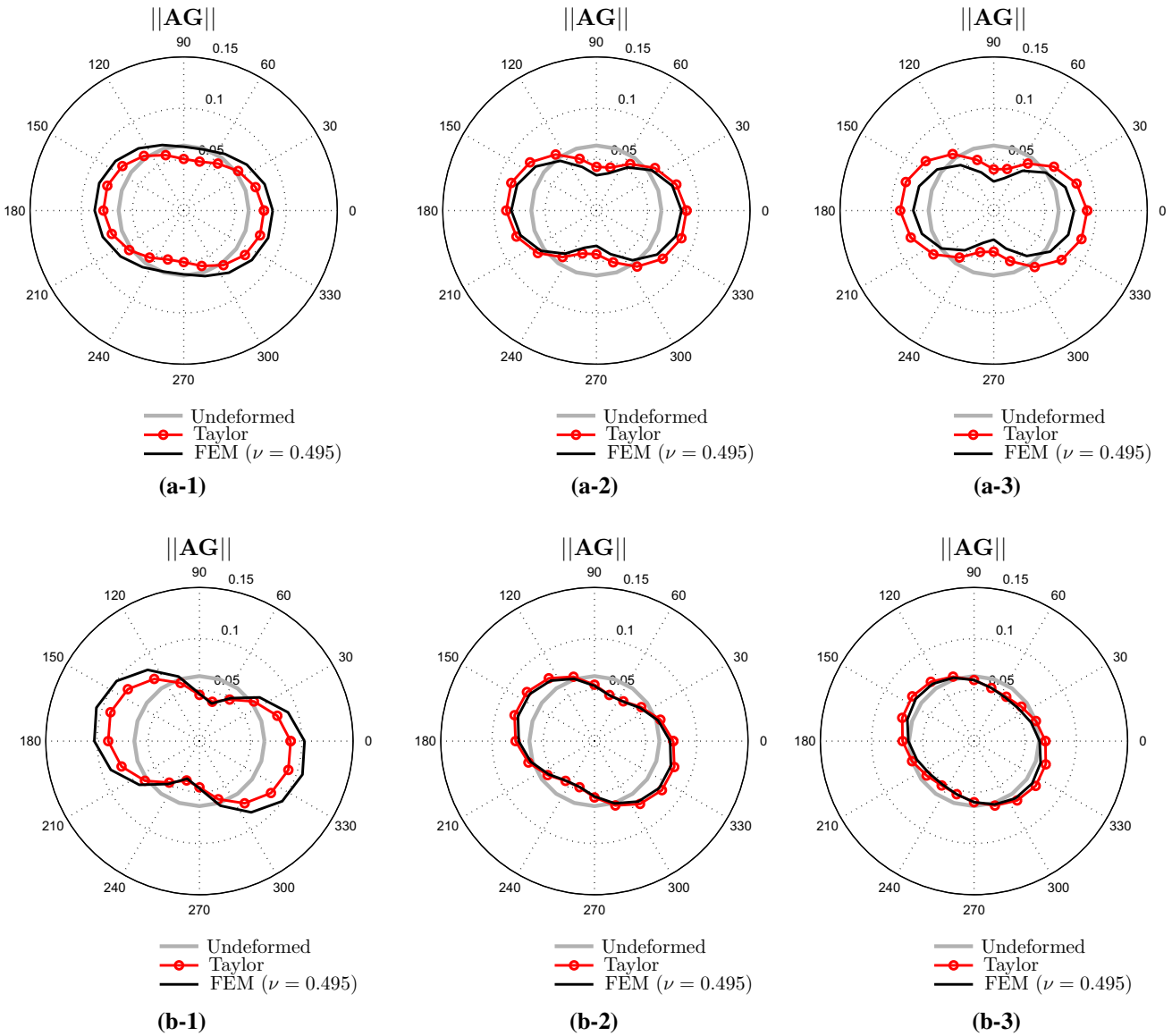

Fig. 17 The macroscopic responses are depicted for shear-stretch combined non-area-preserving deformations with the gradients $\mathbf{F}_s^{1,\gamma}$ (*upper row*) and $\mathbf{F}_s^{2,\gamma}$ (*lower row*) in (4.5). **a-1** $\gamma = -0.2$ ($\det \mathbf{F}_s^{1,\gamma} = 0.857$) **a-2** $\gamma = 0.2$ ($\det \mathbf{F}_s^{1,\gamma} = 1.143$), **a-3** $\gamma = 0.4$ ($\det \mathbf{F}_s^{1,\gamma} = 1.286$), **b-1** $\gamma = -0.29$ ($\det \mathbf{F}_s^{2,\gamma} = 0.880$), **b-2** $\gamma = 0.3$ ($\det \mathbf{F}_s^{2,\gamma} = 1.120$), **b-3** $\gamma = 0.6$ ($\det \mathbf{F}_s^{2,\gamma} = 1.240$)

surface generation algorithm. This sample size effect quickly diminishes with increasing sample size. For larger sample sizes, each sample displays a nearly isotropic response before deformation and different samples display similar anisotropic responses after deformation. These observations correlate with the results in Fig. 10.

5 Conclusion

Lubrication phenomenon is encountered in various applications ranging from industrial to biological. The influence of the microstructure on the macroscopic lubrication response has been of interest in the literature, where homogenization has appeared as one of the most reliable approaches. In this work, the homogenization treatment of hydrodynamic lubrication has been presented in a setting that unifies the stationary, quasi-stationary and unsteady cases. The macroscopic response of the unsteady problem in the case of periodic commensurate microrough surfaces oscillates with a fine-scale time. A time averaging method combined with homogenization has been proposed to deliver an approximate macroscopic response, which is satisfactory for small roughness RMS values and delivers a reason-

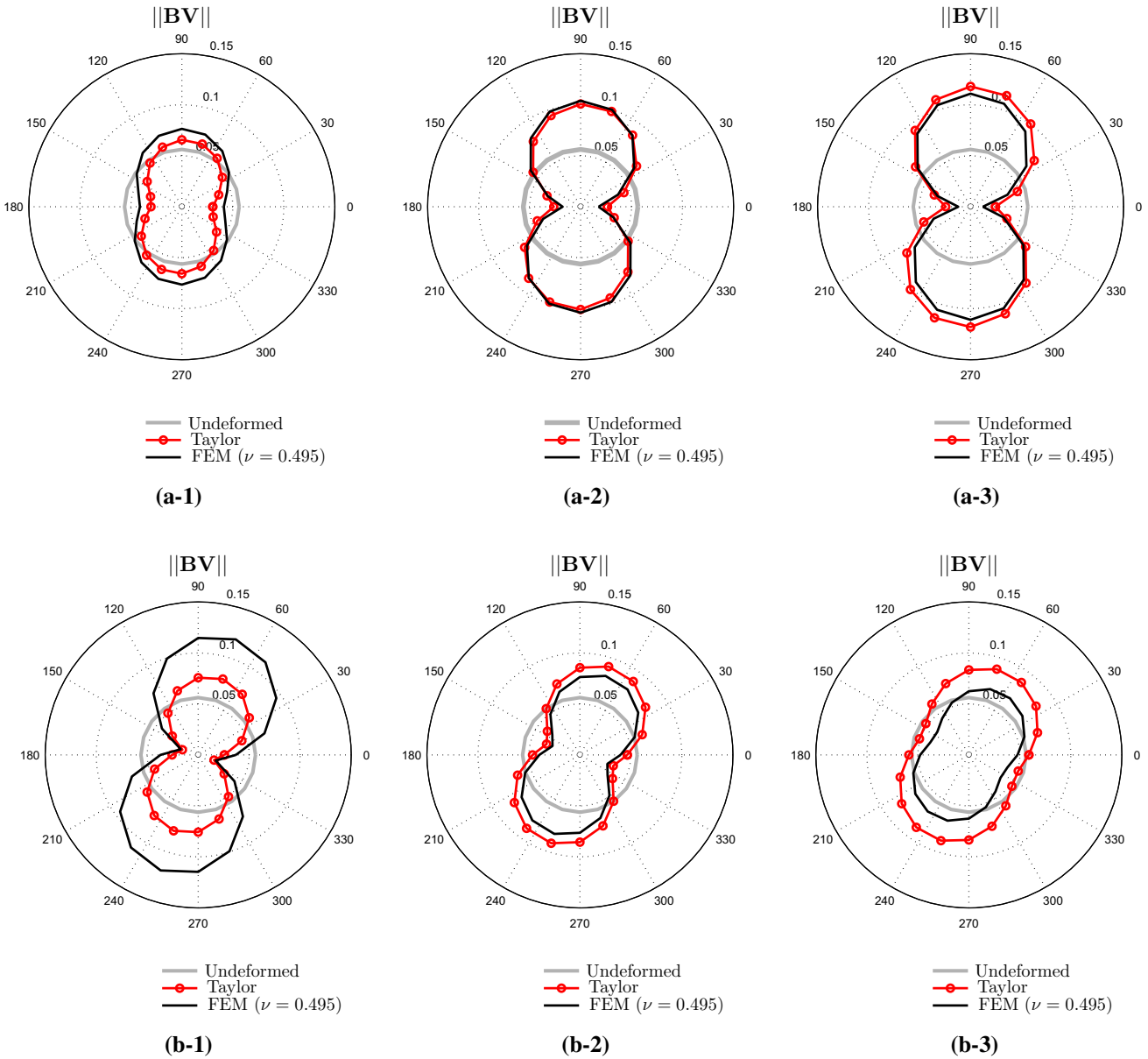

Fig. 18 The macroscopic responses (i.e. the homogenized coefficient tensor $\mathbf{B}$ in this case) are depicted for shear-stretch combined non-area-preserving deformations with the gradients $\mathbf{F}_s^{1,\gamma}$ (*upper row*) and $\mathbf{F}_s^{2,\gamma}$ (*lower row*) in (4.5). **a-1** $\gamma = -0.2$ ($\det \mathbf{F}_s^{1,\gamma} = 0.857$), **a-2** $\gamma = 0.2$ ($\det \mathbf{F}_s^{1,\gamma} = 1.143$), **a-3** $\gamma = 0.4$ ($\det \mathbf{F}_s^{1,\gamma} = 1.286$), **b-1** $\gamma = -0.29$ ($\det \mathbf{F}_s^{2,\gamma} = 0.880$), **b-2** $\gamma = 0.3$ ($\det \mathbf{F}_s^{2,\gamma} = 1.120$), **b-3** $\gamma = 0.6$ ($\det \mathbf{F}_s^{2,\gamma} = 1.240$)

able first order estimation for large roughness RMS. For incommensurate periodic surfaces, it has been observed that the macroscopic response is not a function of the microscopic time. Since most real surfaces are inherently randomly rough and incommensurate, they are expected to also display a time-independent response, which has been verified through numerical investigations. Additionally, it has been shown that ensemble averaging covers time averaging in a statistical sense and hence the unsteady lubrication problem with random microrough surfaces can be considered as quasi-stationary at the microscale, leading to a computationally efficient two-scale analysis framework. Finally, the Taylor assumption has been proposed to further enhance computational efficiency for the time-dependent soft lubrication problem. In particular, the effectiveness of the Taylor assumption has been demonstrated in the case of area-preserving deformations, while further improvement is needed for non-area-preserving deforma-

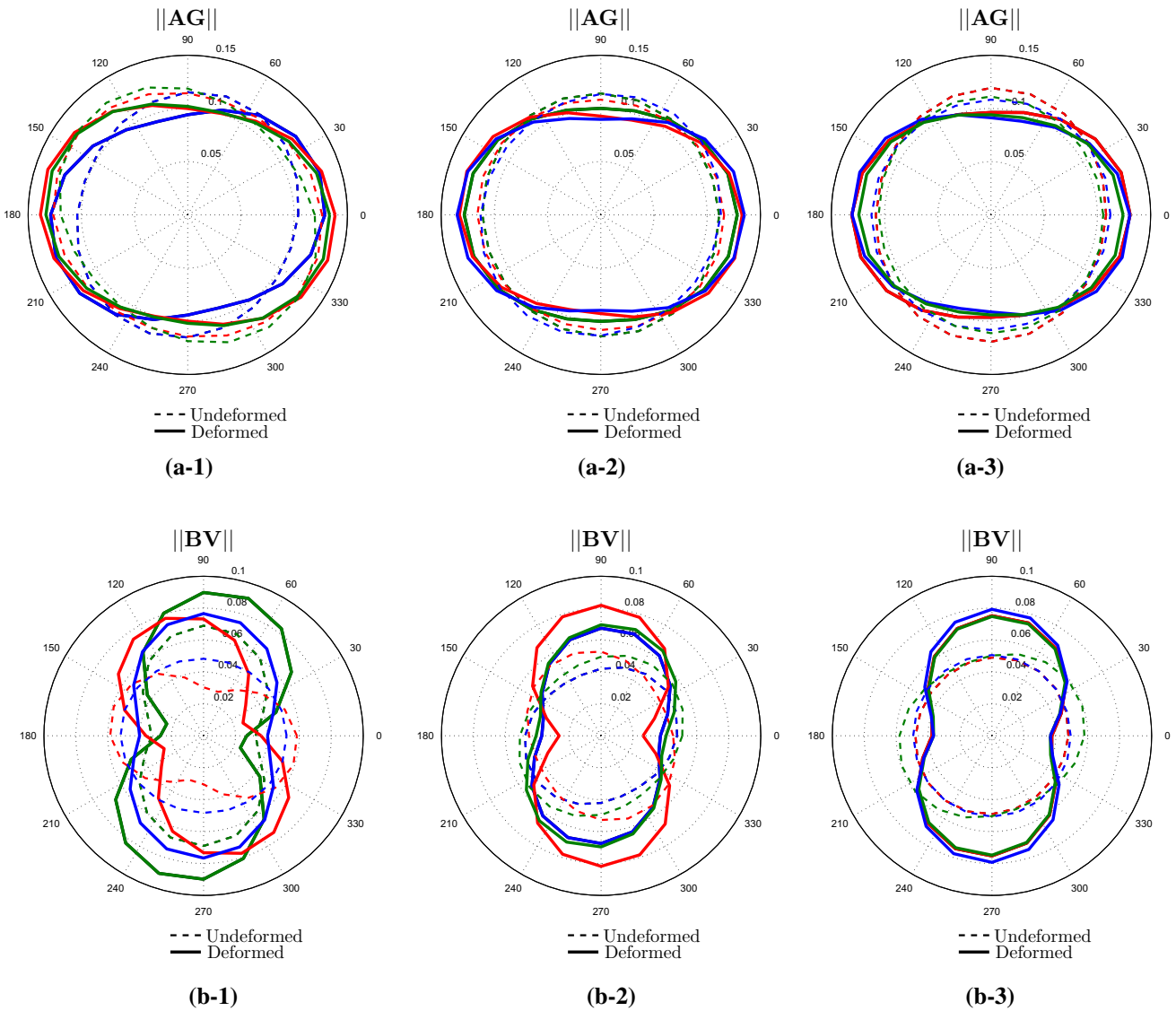

Fig. 19 For different sample sizes of random microrough surfaces and three realizations per sample size, the macroscopic responses are depicted for shear-stretch combined non-area-preserving deformations with the gradient $\mathbf{F}_s^{2,\gamma}$ in (4.5) using $\gamma = 0.3$. The deformation effects are reflected through the Taylor assumption in all cases (**a-1**) Size $= 20 \times 20$. **a-2** Size $= 40 \times 40$, **a-3** Size $= 100 \times 100$, **b-1** Size $= 20 \times 20$, **b-2** Size $= 40 \times 40$, **b-3** Size $= 100 \times 100$

tions. Future work will concentrate on the application of the developed framework to two-scale soft elastohydrodynamic lubrication problems, involving aspects of the macroscopic problem solution, as well as on surface engineering applications, specifically to surface texture design and optimization.

Acknowledgments Support by the Scientific and Technological Research Council of Turkey (TÜBİTAK) under the 1001 Programme (Grant No. 114M406) and by the European Commission under the project *MultiscaleFSI* (Grant No. PCIG10-GA-2011-303577) is gratefully acknowledged.

References

1. Hamrock B, Schmid S, Jacobson B (2004) Fundamentals of fluid film lubrication. CRC Press, Boca Raton
2. Szeri AZ (2011) Fluid film lubrication. Cambridge University Press, Cambridge
3. Reynolds O (1886) On the theory of lubrication and its application to Mr. Beauchamp tower's experiments including and experimental determination of the viscosity of olive oil. Philos Trans R Soc Lond 177:157–234
4. Tabor D, Bowden FP (1950) Friction and lubrication of solids, part I. Oxford University Press, Oxford
5. Jin Z, Dowson D (2005) Elastohydrodynamic lubrication in biological systems. Proc Inst Mech Eng Part J 219:367–380

6. Dowson D, Jin Z (2006) Metal-on-metal hip joint tribology. Proc Inst Mech Eng part H 220:107–118
7. Myant C, Cann P (2013) In contact observation of model synovial fluid lubricating mechanisms. Tribol Int 63:97–104
8. Mattei L, Di Puccio F, Piccigallo B, Ciulli E (2011) Lubrication and wear modeling of artificial hip joints: a review. Tribol Int 44:532–549
9. Dunn AC, Tichy JA, Urue na JM, Sawyer WG (2013) Lubrication regimes in contact lens wear during a blink. Tribol Int 63:45–50
10. Scaraggi M, Persson BNJ (2012) Time-dependent fluid squeeze-out between soft elastic solids with randomly rough surfaces. Tribol Lett 47:409–416
11. Ma C, Zhu H (2011) An optimum design model for textured surface with elliptical-shape dimples under hydrodynamic lubrication. Tribol Int 44:987–995
12. Tala-Ighil N, Fillon M, Maspeyrot P (2011) Effect of textured area on the performance of a hydrodynamic journal bearing. Tribol Int 44:211–219
13. Yuan S, Huang W, Wang X (2011) Orientation effects of micro-grooves on sliding surfaces. Tribol Int 44:1047–1054
14. Scaraggi M (2014) Optimal textures for increasing the load support in a thrust bearing pad geometry. Tribol Lett 53:127–143
15. Bayada G, Ciuperca I, Jai M (2006) Homogenized elliptic equations and variational inequalities with oscillating parameters. application to the study of thin flow behavior with rough surfaces. Nonlinear Anal 7(5):950–996
16. Kane M, Bou-Said B (2004) Comparison of homogenization and direct techniques for the treatment of roughness in incompressible lubrication. J Tribol 126:733–737
17. Kweh CC, Patching MJ, Evans HP, Spindle RW (1992) Simulation of elastohydrodynamic contact between rough surfaces. J Tribol 114:412–419
18. Eng J, Greenwood JA, Espejel GE (1994) The behavior of transverse roughness in EHL contact. Proc Inst Mech Eng Part J 208:121–132
19. Tzeng ST, Saibel E (1967) Surface roughness effect on slider lubrication. ASLE Trans 10:334–337
20. Christensen H, Tonder K (1971) The hydrodynamic lubrication of rough bearing surfaces of finite width. J Lubr Technol Trans ASME 93:324–330
21. Patir N, Cheng HS (1978) An average flow model for determining effects of three-dimensional roughness on partial hydrodynamic lubrication. J Lubr Technol Trans ASME 100:12–17
22. Patir N, Cheng HS (1979) Application of average flow model to lubrication between rough sliding surfaces. J Lubr Technol Trans ASME 101:220–230
23. Tripp JH (1983) Surface roughness effects in hydrodynamic lubrication: the flow factor method. J Lubr Technol Trans ASME 105:458–463
24. Elrod HG (1973) Thin film lubrication theory for newtonian fluids with surface possessing striated roughness or grooving. J Lubr Technol Trans ASME 95:484–489
25. Almqvist A, Fabricius J, Spencer A (2011) Similarities and differences between the flow factor method by Patir and Cheng and homogenization. J Tribol 133(3):031702
26. Sun D-C (1978) On the effects of two-dimensional Reynolds roughness in hydrodynamic lubrication. Proc R Soc Lond Ser A Math Phys Sci 364:89–106
27. Elrod HG (1979) A general theory for laminar lubrication with Reynolds roughness. J Lubr Technol Trans ASME 101:8–14
28. Almqvist A, Dasht J (2006) The homogenization process of the Reynolds equation describing compressible liquid flow. Tribol Int 39:994–1002
29. Essel EK (2008) Homogenization of Reynolds equations and of some parabolic problems via Rothe's method. PhD thesis, Luleå University of Technology
30. Fabricius J (2008) Homogenization of some problems in hydrodynamic lubrication involving rough boundaries. PhD thesis, Luleå University of Technology
31. Almqvist A, Lukkassen D, Meidell A, Wall P (2007) New concepts of homogenization applied in rough surface hydrodynamic lubrication. Int J Eng Sci 45:139–154
32. Lukkassen D, Meidell A, Wall P (2007) Homogenization of some variational problems connected to the theory of lubrication. Int J Eng Sci 47:153–162
33. Buscaglia GC, Jai M (2003) Homogenization of the generalized Reynolds equation. Mec Comput 22:41–56
34. Almqvist A, Essel EK, Fabricius J, Wall P (2008) Variational bounds applied to unstationary hydrodynamic lubrication. Int J Eng Sci 46:891–906
35. Jai M (1995) Homogenization and two-scale convergence of the compressible Reynolds lubrication equation modeling the flying characteristics of a rough magnetic head over a rough rigid-disk surface. Math Model Numer Anal 29:199–233
36. Jai M, Bou-Said B (2002) A comparison of homogenization and averaging techniques for the treatment of roughness in slip-flow-modified Reynolds equation. J Tribol 124:327–335
37. Dowson D (1995) Elastohydrodynamic and micro-elastohydrodynamic lubrication. Wear 190:125–138
38. Shi F, Salant RF (2000) A mixed soft elastohydrodynamic lubrication model with interasperity cavitation and surface shear deformation. J Tribol 122:308–316
39. Bayada G, Martin S, Vazquez C (2006) Micro-roughness effects in (elasto)hydrodynamic lubrication including a mass-flow preserving cavitation model. Tribol Int 39:1707–1718
40. Budt M, Temizer İ, Wriggers P (2012) A computational homogenization framework for soft elastohydrodynamic lubrication. Comput Mech 49:749–767
41. Arghir M, Roucou N, Helene M, Frene J (2003) Theoretical analysis of the incompressible laminar flow in a macro-roughness cell. J Tribol 125:309–318
42. Almqvist T, Larsson R (2004) Some remarks on the validity of Reynolds equation in the modeling of lubricant film flows on the surface roughness scale. J Tribol 126:703–709
43. Sahlin F, Glavatskih SB, Almqvist T, Larsson R (2005) Two-dimensional CFD-analysis of micro-patterned surfaces in hydrodynamic lubrication. J Tribol 127:96–102
44. de Kraker A, van Ostayen RAJ, van Beek A, Rixen DJ (2007) A multiscale method modeling surface texture effects. J Tribol 129:221–230
45. Dobrica MB, Fillon M (2009) About the validity of Reynolds equation and inertia effects in textured sliders of infinite width. Proc IMechE Vol 223 Part J 223:69–78
46. Bayada G, Chambat M (1989) Homogenization of the Stokes system in a thin film flow with rapidly varying thickness. Math Model Numer Anal 23:205–234
47. Stupkiewicz S, Marciniszyn A (2009) Elastohydrodynamic lubrication and finite configuration changes in reciprocating elastomeric seals. Tribol Int 42:615–627
48. Prat M, Plouraboué F, Letalleur N (2002) Averaged Reynolds equation for flows between rough surfaces in sliding motion. Transp Porous Media 48:291–313
49. Ringlein J, Robbins MO (2004) Understanding and illustrating the atomic origins of friction. Am J Phys 72(7):884–891
50. Garcia N, Stoll E (1984) Monte Carlo calculation for electromagnetic-wave scattering from random rough surfaces. Phys Rev Lett 52(20):1798–1801
51. Torquato S (2001) Random heterogeneous materials. Springer, New York
52. Temizer I (2011) Thermomechanical contact homogenization with random rough surfaces and microscopic contact resistance. Tribol Int 44:114–124

53. Beran MJ (1968) Statistical continuum theories. Wiley, New York
54. Nemat-Nasser S, Hori M (1991) Micromechanics: overall properties of heterogeneous materials. North-Holland, Amsterdam
55. Scaraggi M, Carbone G, Persson BNJ, Dini D (2011) Lubrication in soft rough contacts: a novel homogenization approach part I—theory. Soft Matter 7:10395–10406
56. Scaraggi M, Carbone G, Dini D (2011) Lubrication in soft rough contacts: a novel homogenization approach part II—discussion. Soft Matter 7:10407–10416